MANTLE SOURCE REGIONS AND MAGMA EVOLUTION ALONG THE JUAN DE FUCA RIDGE, PACIFIC OCEAN

Senior Thesis

Submitted in partial fulfillment of the requirements for the

Bachelor of Science Degree

at The Ohio State University

By

William D. Evarts

The Ohio State University

2016

Approved by

Dr. Michael Barton, Advisor

School of Earth Sciences

TABLE OF CONTENTS

ABSTRACT

Magmas are intruded and erupted along the axes of mid-ocean ridges. As part of a larger effort to understand crustal accretion at these plate boundaries, we are studying the petrology and geochemistry of erupted lavas to characterize magma plumbing systems and to determine the processes that occur during magma ascent and evolution. The focus of this research is the Juan de Fuca Ridge (JdF) which extends from the Blanco fracture zone at ~ 44.5° N to a triple junction with the Nootka Fault and the Sovanco fracture zone at 48.7° N in the northeastern Pacific ocean. Petrologic studies indicate that partial crystallization of magmas occurs in reservoirs located at various depths in the crust, and magmas evolve via crystallization in these reservoirs. A study of the trace element geochemistry of erupted lavas was undertaken to ascertain whether crystallization is the only process occurring during magma evolution and to probe the mantle source regions of the magmas. Geochemical data were compiled from Gale et al. (2013), and individual analyses were normalized to the composition of average Normal Mid-Ocean Ridge basalt (NMORB), CI chondrites, and the primitive mantle to aid interpretation of geochemical variations. Ratios of La/Sm, K/U, K/Ti, and K/P were calculated and plotted against latitude in order to determine the extent of crustal assimilation affecting the magmas, as well as to gain insight into the enrichment of the mantle sources. Furthermore, Na_8 values from Scott et al. (2012) were examined to determine if different regions of the ridge had undergone different degrees of mantle melting. From this information, we determined that there are at least two mantle sources for the Juan de Fuca ridge: a Depleted MORB Mantle (DMM) source in the south, and a Normal Mid-Ocean Ridge Basalt (NMORB) source in the north. In addition, trace element data normalized to N-MORB show similar patterns of relative enrichment within ridges, but with large ranges of enrichment among different samples, particularly in segments 1, 2, 3, and 4, indicating that extensive fractional crystallization has occurred in those regions. Strontium anomalies also indicate that plagioclase played a major role in crystallization.

ACKNOWLEDGEMENTS

I would like to thank my research advisor, Dr. Michael Barton, for his incredible guidance, wisdom, and patience with me throughout my research project. I would also like to extend my gratitude to Jameson Scott for sharing his knowledge, skills, and humor with me, and to Dr. Anne Carey for her help in ensuring that this thesis was actually completed. In addition, I would like to thank all of my professors, advisors, and fellow students in the Ohio State School of Earth Sciences for keeping me engaged, positive, and for teaching me more than I ever imagined about geology.

Finally, I will forever be grateful to my parents, my girlfriend, and the rest of my family. Without their interminable and unwavering support and encouragement, this project would never have been completed.

LIST OF FIGURES

LIST OF TABLES

INTRODUCTION

The Juan de Fuca ridge is a mid-ocean ridge in the northeastern Pacific Ocean off the coast of Oregon, Washington, and British Columbia. This ridge is being studied as part of a larger effort to examine the processes by which magma upwells to form new oceanic crust at mid-ocean ridges, and the depths at which those processes occur. In this study, we analyzed the geochemistry of samples from the Juan de Fuca ridge in order to determine the extent to which crustal assimilation and fractional crystallization affect the magmas as they ascend to the ridge, and to unearth as much information as possible about the magma source regions for the ridge.

This study primarily focuses on using trace element geochemistry to investigate the sources and evolution of the ridge magmas. Despite their low abundance, trace elements can provide a substantial amount of information about the geochemistry of a system. For many trace elements, the degree of variation in concentrations may be orders of magnitude larger than the variations in concentrations of major oxides for the same sample (White, 2013). For this reason, trace elements can be useful for examining processes that alter the composition of a rock, like fractional crystallization and assimilation. In addition, there are many more trace elements in any system than there are major oxides. Though major elements may account for over 99% of a sample, the trace elements each possess chemical properties such that their individual variations provide unique geochemical information (White, 2013). The range of information that can be provided by those trace elements is also extensive, and because trace elements often show a strong preference for different phases, their variations can provide information about geochemical processes that cannot be discerned from major elements. Finally, trace element behavior is generally simpler than the behavior of major elements, allowing for comparatively simple modelling of natural processes. For these reasons, trace elements are ideal for examining the processes affecting magmas at mid-ocean ridges and their sources.

GEOLOGIC SETTING

Mid-Ocean Ridges

The mid-ocean ridge (MOR) system is the longest continuous mountain range on earth and represents the site of generation of new lithosphere. Buoyant magma upwells and erupts onto the seafloor or crystallizes below the surface, creating new oceanic crust. The newly formed lithospheric plates spread away from the ridges accounting for movement of the continents with time.

The composition of mid-ocean ridge basalts (MORB) can be studied in order to determine the amount of fractional crystallization they have undergone, the degree of melting taking place in the mantle, and the composition of the mantle source region. Petrologic studies indicate that partial crystallization of magmas occurs in reservoirs located at various depths in the crust below MORs, and that magmas evolve via crystallization in these reservoirs.

The Juan de Fuca Ridge

The Juan de Fuca Ridge is an intermediate-spreading (~6 cm yr^{-1}) MOR that extends from the Blanco fracture zone at ~44.5°N to a triple junction with the Nootka Fault and the Sovanco fracture zone at 48.7°N in the northeastern Pacific Ocean, dividing the Pacific Plate from the Juan de Fuca plate.

Axial Seamount

The Juan de Fuca ridge contains a notable submarine volcano known as the Axial Seamount. This seamount is located at the intersection between the ridge and the Cobb-Eickelberg Seamount chain to the west of the ridge. The Axial Seamount is also the topographic high of the ridge, at about 1700 m below sea level, while the rest of the ridge has little topographic deviation, varying from 2344 m to about 2500 m below sea level.

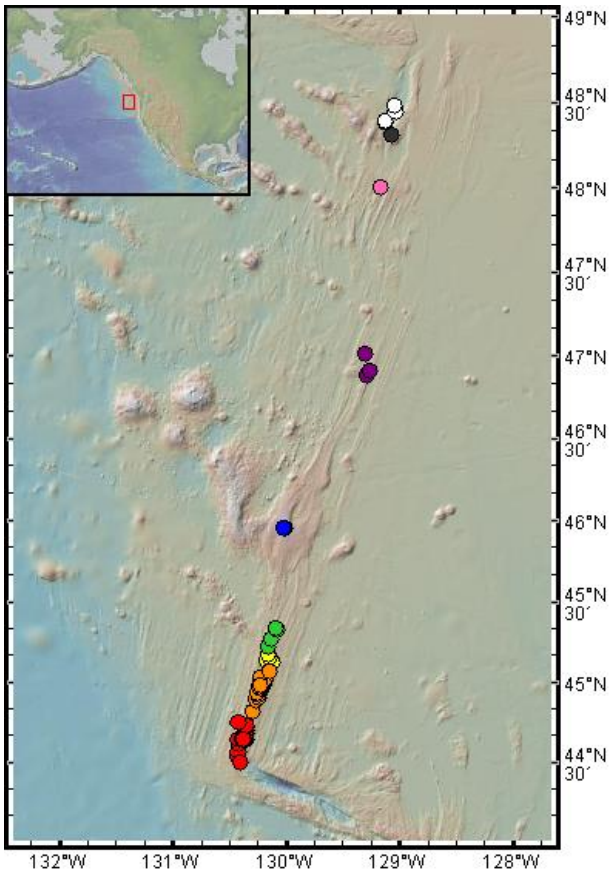

Figure 1. Location of samples (colored dots) on the Juan de Fuca Ridge. Colors represent different ridge segments as defined in Table A1. Created using GeoMapApp.

METHODS

Data for this study were primarily taken from the catalog of ridge basalt analyses published by Gale et al. (2013), which contained 102 samples for the Juan de Fuca ridge. The data consisted of whole rock samples retrieved via dredging and basaltic glasses (see Tables D3 and D4 for these data). The Juan de Fuca ridge was then divided into 22 segments by latitude using natural grouping by proximity of samples. The dataset contained samples for 9 of our 22 segments. Specific ranges for latitude and longitude can be found in Table A1. The data were analyzed using Microsoft Excel and the Cohort statistical plotting package.

Normalization to Trace and Rare-Earth Elements

After we separated the samples into appropriate segments, trace element data from Gale et al. (2013) were normalized in order to aid in the comparison of samples within and between segments. Each segment was normalized to three different compositions. Rare-earth elements were normalized to CI Chondrite compositions (from McDonough and Sun, 1995), and rare earths and other trace elements were normalized to both primordial mantle composition (from Sun and McDonough, 1989) and average normal mid-ocean ridge basalt (or N-MORB) compositions (from Gale et al., 2013). See Table A2 for normalization values.

We removed any samples that did not contain complete sets of data for the trace elements being examined. The remaining Gale et al. (2013) data consisted of 43 samples for the N-MORB normalized data, 48 samples for the CI chondrite normalized data, and 46 samples for the primordial mantle normalized data. The normalized data were plotted by segment and analyzed. See Figures B2, B3, and B4 for plots of normalized data.

Samples can be classified as enriched or depleted based on Primitive Mantle normalizations as defined by Gale et al. (2013). A sample was categorized as Enriched MORB (E-MORB) if the La/Sm mass ratio was greater than 1.5, and as Depleted MORB (D-MORB) if the La/Sm mass ratio was less than 0.8. If the La/Sm mass ratio was between 0.8 and 1.5, the sample was considered to be N-MORB. Only data for samples that included values for both La and Sm could be used, so samples with incomplete data were removed from consideration, leaving 61 samples to be used for this calculation. See Figure C5 for a plot of La/Sm against latitude.

The N-MORB normalization was also useful for determining enrichment, since it allowed for the straightforward comparison of normalized plots (Figure B3) to plots of what would be expected from a normal MORB mantle source. The difference in pattern among expected E-MORB, D-MORB, and N-MORB values is predicted to be most obvious in the incompatible elements cesium, rubidium, and barium, because those elements are preferentially concentrated in the melt phase of the magma during fractional crystallization.

Na_8 Analysis

Na_8 analysis uses linear regression to correct Na_2O concentrations to 8 wt% MgO. This effectively removes the influence of fractionation on Na_2O in the magmas, and can be used to probe the conditions in the magma source regions of a ridge. Since Na_2O behaves incompatibly, it preferentially enters the melt and become more diluted with higher degrees of melting. Therefore, a mantle source region with a high degree of melting will have a low Na8 value. This inverse correlation between degree of melting and Na8 can provide valuable insight into the temperature and conditions of the magma source (Klein and Langmuir, 1987). We used Na_8 values from Scott et al. (2012) for our study.

Element Ratio Analysis

Major oxide data were taken from Gale et al. (2013), and the ratios K/Ti, K/P, and K/U were calculated. The ratios K/Ti and K/P can be used as evidence for crustal assimilation occurring during magma evolution (Wanless et al., 2010). The ratio K/U can give some insight into the enrichment of the magma in different regions of the ridge, with higher K/U values corresponding to more enriched samples (Gale et al., 2013). Together, these three ratios can provide evidence for homogeneity or heterogeneity along the ridge. The ratios were all plotted versus latitude without dividing them into segments in order to visualize the overall homogeneity or heterogeneity of the ridge. See Figures C7, C8, and C9 for these plots.

RESULTS

Normalized Plots

Analysis of the normalized plots shows different regions of enrichment along the ridge. Inspection of the N-MORB normalized plots (Figure B3) reveals that the southern segments of the ridge have a distinct depletion in the incompatible elements cesium, rubidium, and barium. The segments farther north do not show this depletion on N-MORB plots.

Depletion in the southern segments is less clear on the plot of La/Sm ratios (Figure C5). Based on the La/Sm plot, there are samples depleted in incompatible elements in nearly all regions of the ridge. However, there is a large spread of La/Sm values, especially near the northern sections of the ridge near the Sovanco fracture zone. La/Sm values in the southern sections of the ridge are more concentrated around a value of 0.8, indicating more depleted lavas in that region.

Trace element data, especially in segments 1, 2, 3, 4, and 5 (Figure B3), show similar patterns of relative enrichments and depletions within a segment, causing the data from different samples in a segment to appear sub-parallel on the normalization plots. However, some samples are more enriched overall than others within a given segment. This is particularly evident in segment 1 (Figure B3), near the Blanco fracture zone at the southern end of the ridge. In this segment, some samples are enriched by nearly an order of magnitude relative to others in the same segment, but most samples still show the same general patterns of element enrichment.

Anomalous strontium values—and to a lesser degree, europium and barium values—are evident in some segments, particularly in segments 1, 3, 14, and 21. This can most easily be seen in the distinct drop in concentrations for those elements in the plots of trace elements normalized to N-MORB (Figure B3).

Na_8 and Element Ratio Analysis

Na_8 values ranged from 1.54 to 3.32 along the ridge, with no segment of the ridge having particularly high or low values (see Figure C6). This indicates a consistent degree of melting along the ridge and a relatively constant temperature of melt.

Unfortunately, after removing samples with incomplete data, there remained only 30 samples with calculated K/U ratios, 75 samples with calculated K/P ratios, and 84 samples with calculated K/Ti ratios. North of segment 4, only three K/P ratios and only two K/U ratios could be calculated. There were no data to calculate the K/U ratio above a latitude of 47°N.

The samples for which ratios could be calculated show a large range of values in the southern segments of the ridge, particularly in the ratio K/U. The 11 samples north of segment 4 had K/Ti ratios calculated, and they do not show a significant variation from the K/Ti ratios calculated in the southern segments (see Figures C7, C8, and C9).

DISCUSSION

The differences in observations of incompatible elements indicate that there are at least two mantle source regions for the ridge: a Depleted MORB Mantle (DMM) source in the south, and a Normal Mid-Ocean Ridge Basalt (NMORB) source in the north. This can most easily be seen by comparison of the incompatible elements in the plots of trace elements normalized to N-MORB. The depletion is especially evident in segments 1, 2, 3, and 4 of Figure B3. La/Sm ratios also support the hypothesis that the southern regions of the ridge are more depleted than the northern regions (Figure C5).

In addition, since there is little variation in the degree of melting along the ridge, as indicated by the roughly constant Na_8 data (Figure C6), the observed geochemical variations must be explained by processes unrelated to the degree of melting, such as different mantle source regions.

The calculated element ratios, particularly K/Ti (Figure C8), show little change between the southern and northern segments of the ridge, which suggests that there is little change in the amount of crustal assimilation occurring on different segments. However, due to the lack of data in the northern segments, any firm conclusion is premature.

On the normalization plots (Figure B3), similar patterns of relative enrichment are present, but some segments show a large range of enrichment among different samples. This is consistent with magma evolution via fractional crystallization, wherein magmas become more enriched as evolution progresses, but relative enrichments of trace elements do not change drastically. This pattern is present in the southernmost segments (segments 1, 2, 3, and 4), but is most evident in segment 1 (Figure B3). More extensive fractional crystallization suggests that there may be more pooling of magma in the crust during ascent in those regions.

Finally, the anomalous strontium values in some segments—particularly segments 1, 3, 14, and 21 (Figure B3)—suggest that the crystallization of plagioclase played an important role in magma evolution in those segments. Because strontium can readily substitute for calcium in plagioclase, a magma can become depleted in strontium as plagioclase crystallizes, and this depletion would be expected to appear similar to the anomalies in Figure B3.

CONCLUSIONS

Contrasting observations in incompatible elements on different segments of the Juan de Fuca ridge show that there are at least two different mantle source regions for the ridge: a Depleted MORB Mantle (DMM) source in the south, and a Normal Mid-Ocean Ridge Basalt (NMORB) source in the north. This is supported by differences in La/Sm ratios in those regions. Furthermore, K/Ti ratios and Na_8 results show that observed geochemical differences cannot be explained by differences in degree of assimilation or melting of the crust. In addition, trace element data normalized to N-MORB show similar patterns of relative enrichment within ridges, but with large ranges of enrichment among different samples, particularly in segments 1, 2, 3, and 4. These patterns indicate that extensive fractional crystallization has occurred in those regions, and may suggest that there is more pooling of magma in the crust in the southern region of the ridge. Finally, anomalous strontium values—particularly in segments 1, 3, 14, and 21—suggest that the crystallization of plagioclase played an important role in magma evolution.

SUGGESTIONS FOR FUTURE RESEARCH

The data used for this study were extensive for the most southerly segments of the ridge, but were lacking in all other regions. In order to constrain the magma source regions and processes of magma evolution under the Juan de Fuca ridge, a more complete dataset needs to be analyzed. This would require the collection of more samples from the ridge by dredging or other methods. A more comprehensive dataset may result in different conclusions about those regions. In addition, an isotopic analysis of samples from the ridge might provide more insight into the degree of crustal assimilation affecting the ridge. $\delta^{18}O$ data, coupled with the isotopic ratios $^{87}Sr/^{86}Sr$ and $^{143}Nd/^{144}Nd$, can be used as a gauge of crustal contamination in a magma (Dallai et al., 2003).

REFERENCES CITED

Dallai, L., Ghezzo, C., and Sharp, Z., 2003, Oxygen isotope evidence for crustal assimilation and magma mixing in the Granite Harbour Intrusives, Northern Victoria Land, Antarctica: Lithos, v. 67, no. 1-2, p. 135–151. doi: 10.1016/s0024-4937(02)00267-0.

Gale, A., Dalton, C.A., Langmuir, C.H., Su, Y., and Schilling, J.G., 2013, The mean composition of ocean ridge basalts: Geochem. Geophys. Geosyst., v. 14, p. 489-518. doi:10.1029/2012GC004334

Klein, E.M., and Langmuir, C.H., 1987, Global correlations of ocean ridge basalt chemistry with axial depth and crustal thickness: J. Geophys. Res. Journal of Geophysical Research, v. 92, p. 8089. doi:10.1029/jb092ib08p08089.

McDonough, W.F., and Sun, S.-s., 1995, The composition of the Earth: Chemical Geology, v. 120, p. 223-253. doi:10.1016/0009-2541(94)00140-4.

Scott, J.L., Kelley, D.F., Barton, M., 2012, Petrological constraints on magma plumbing systems along the Reykjanes and Juan de Fuca ridges: 2012 Fall Meeting, AGU, San Francisco, California.

Sun, S.-s., McDonough, W.F., 1989, Chemical and isotopic systematics of oceanic basalts: implications for mantle composition and processes: Geological Society, v. 42, p. 313-345. doi:10.1144/GSL.SP.1989.042.01.19

Wanless, V.D., Perfit, M.R., Ridley, W.I., Klein, E., 2010, Dacite petrogenesis on mid-ocean ridges: Evidence for oceanic crustal melting and assimilation: Journal of Petrology, v. 51, p.2377-2410. doi:10.1093/petrology/egq056.

White, W.M., 2013, Geochemistry: John Wiley & Sons, Hoboken, NJ, p. 259-308.

APPENDICES

Appendix A: Tables

Table A1. Segments as defined by ranges of latitude and longitude, and the colors used for sample locations on Figure 1.

Segment	Latitude Range	Longitude Range	Color
1	44.540°N - 44.760°N	130.500°W - 130.280°W	Red
2	44.820°N - 45.068°N	130.407°W - 130.147°W	Orange
3	45.130°N - 45.170°N	130.167°W - 130.120°W	Yellow
4	45.220°N - 45.333°N	130.160°W - 130.075°W	Green
8	45.863°N - 46.000°N	130.060°W - 129.970°W	Blue
14	46.862°N - 47.208°N	129.300°W - 129.124°W	Purple
19	47.813°N - 48.200°N	129.335°W - 128.978°W	Pink
20	48.167°N - 48.315°N	129.227°W - 129.022°W	Black
21	48.383°N - 48.517°N	129.125°W - 128.917°W	White

Table A2. Values for normalizations of trace element data, in parts per million.

	CI Chondrite	NMORB	Primitive Mantle
Cs		0.024	0.0079
Rb		1.84	0.635
Ba		19.6	6.989
Th		0.252	0.085
U		0.083	0.021
Nb		3.62	0.713
Ta		0.24	0.041
La	0.237	4.19	0.687
Ce	0.613	12.42	1.775
Pb		0.51	0.071
Pr	0.0928	1.98	0.276
Sr		128	21.1
Nd	0.457	10.66	1.354
Zr		101.9	11.2
Hf		2.46	0.309
Sm	0.148	3.48	0.444
Eu	0.0563	1.26	0.168
Gd	0.199	4.55	0.596
Tb	0.0361	0.82	0.108
Dy	0.246	5.5	0.737
Y		33.2	4.55
Ho	0.0546	1.18	0.164
Er	0.16	3.42	0.48
Yb	0.161	3.28	0.493
Lu	0.0246	0.48	0.074

Appendix B: Trace Element Normalization Plots

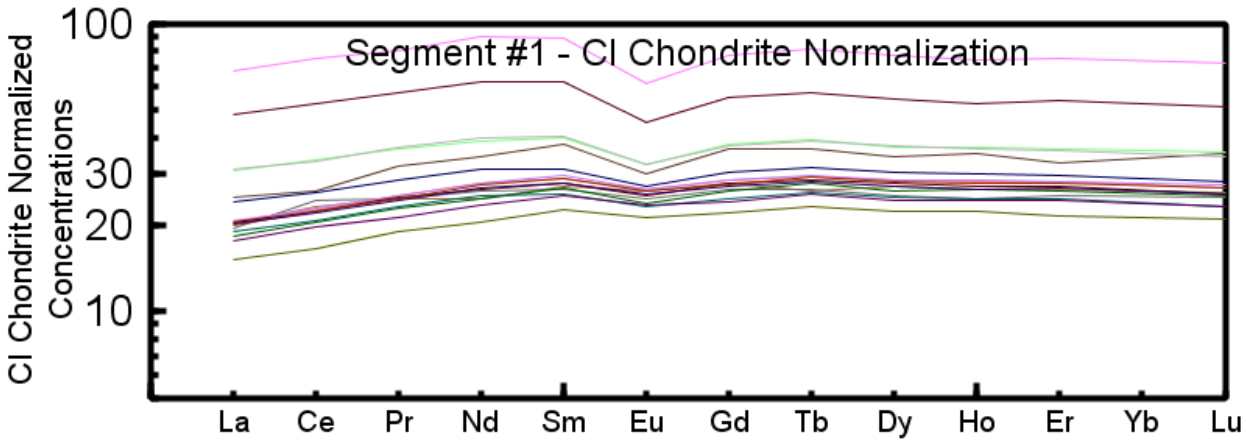

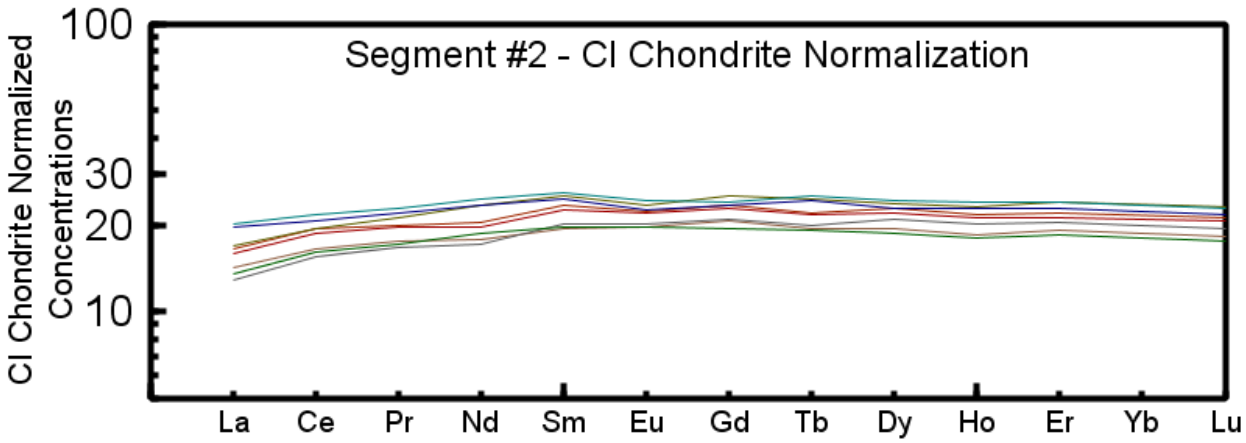

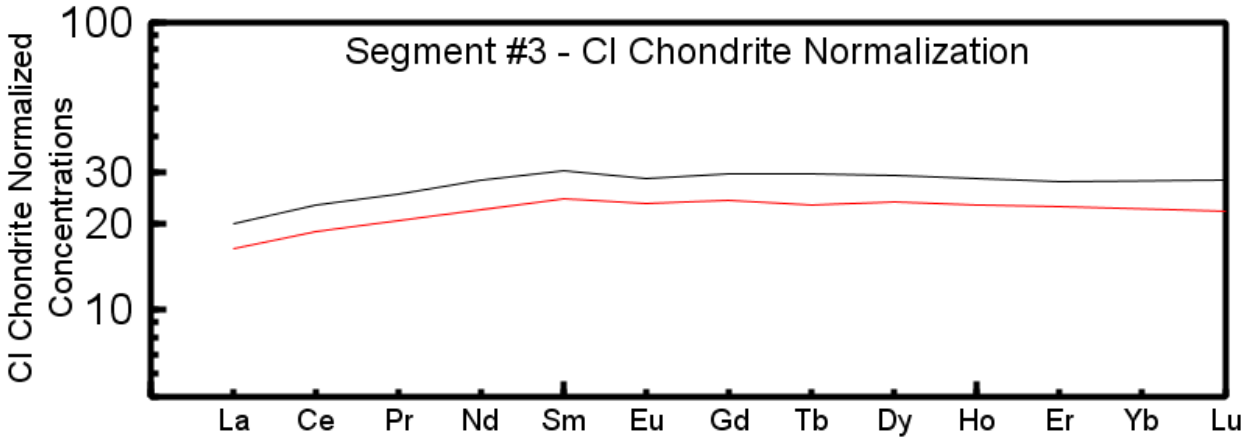

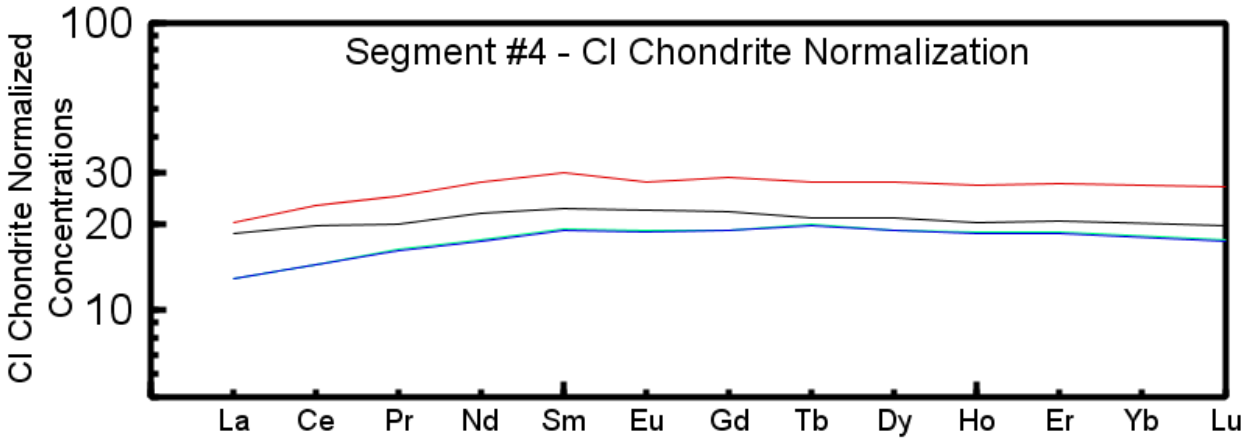
Segment #4 - CI Chondrite Normalization
CI Chondrite Normalized Concentrations
100
30
20
10
La
Ce
Pr
Nd
Sm
Eu
Gd
Tb
Dy
Ho
Er
Yb
Lu

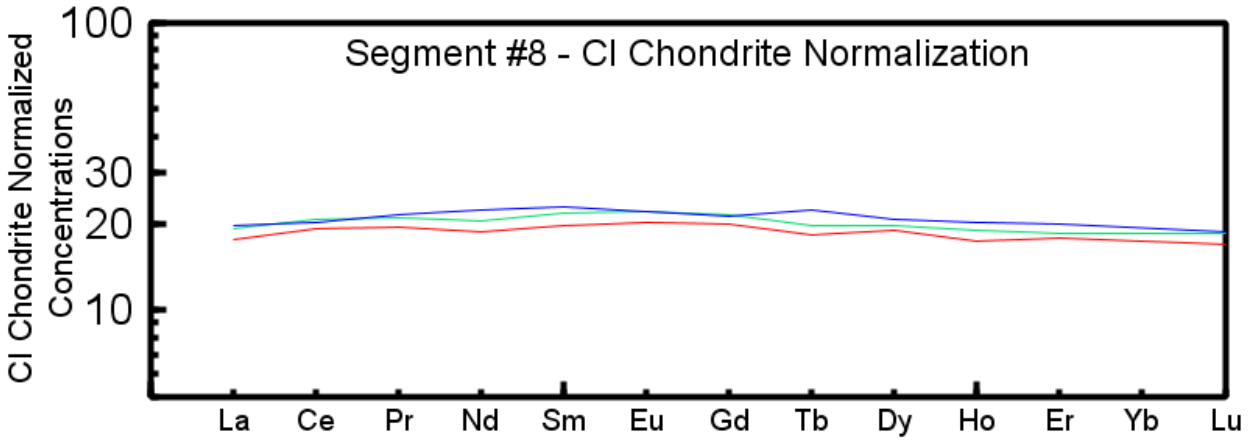
Segment #8 - CI Chondrite Normalization
CI Chondrite Normalized Concentrations
100
30
20
10
La
Ce
Pr
Nd
Sm
Eu
Gd
Tb
Dy
Ho
Er
Yb
Lu

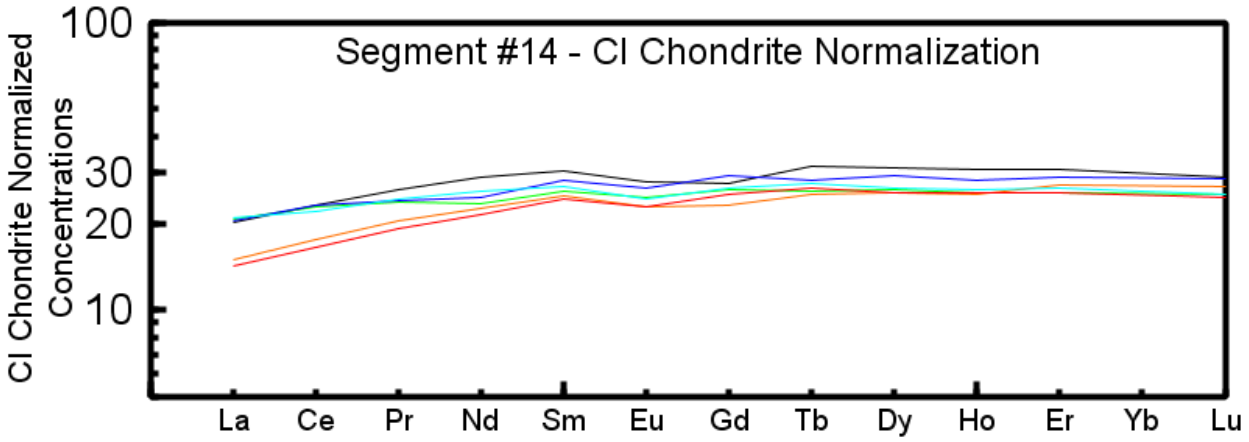
Segment #14 - CI Chondrite Normalization
CI Chondrite Normalized Concentrations
100
30
20
10
La
Ce
Pr
Nd
Sm
Eu
Gd
Tb
Dy
Ho
Er
Yb
Lu

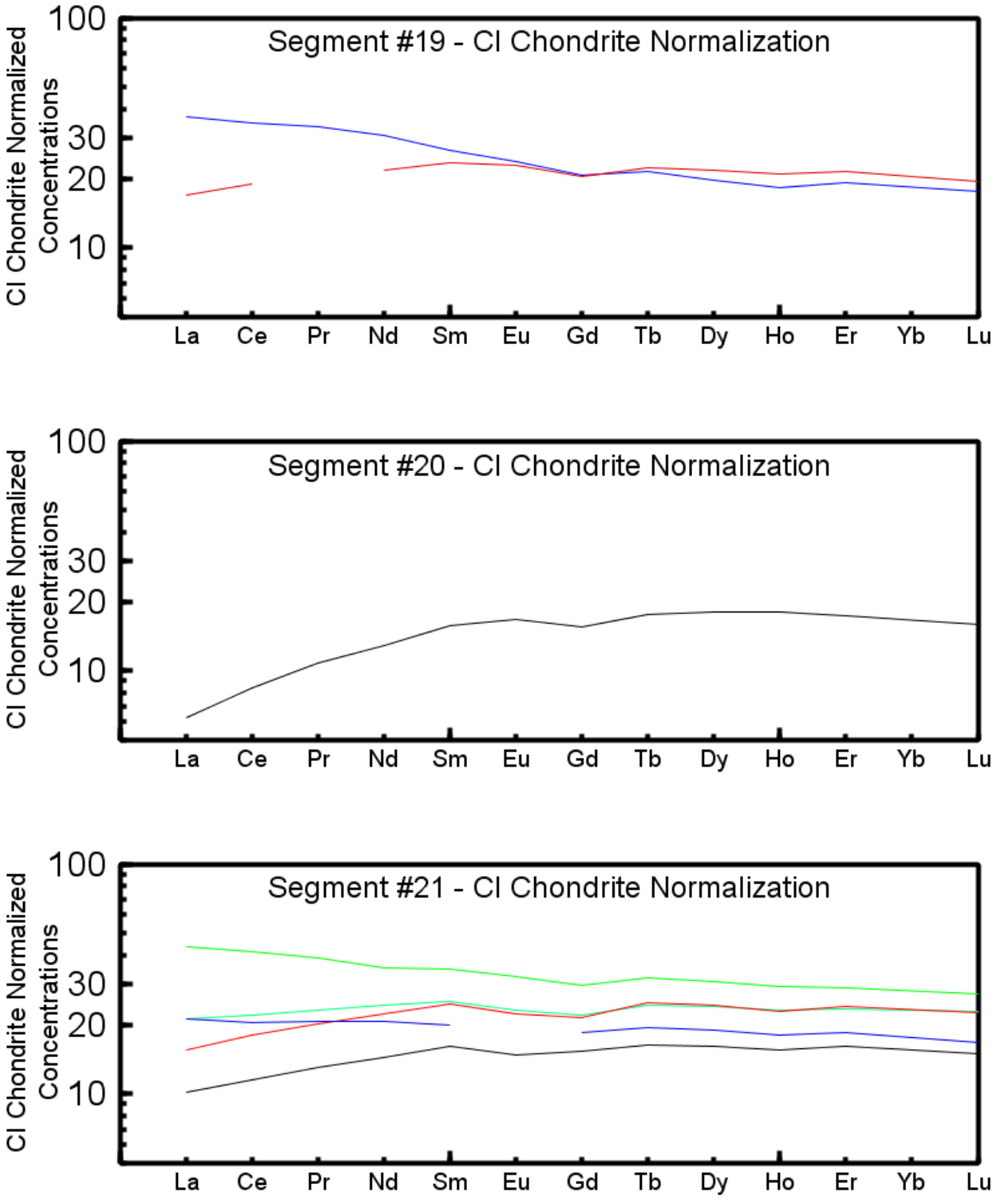

Figure B2. Segmented Gale et al. (2013) rare earth element data, normalized to CI Chondrite.

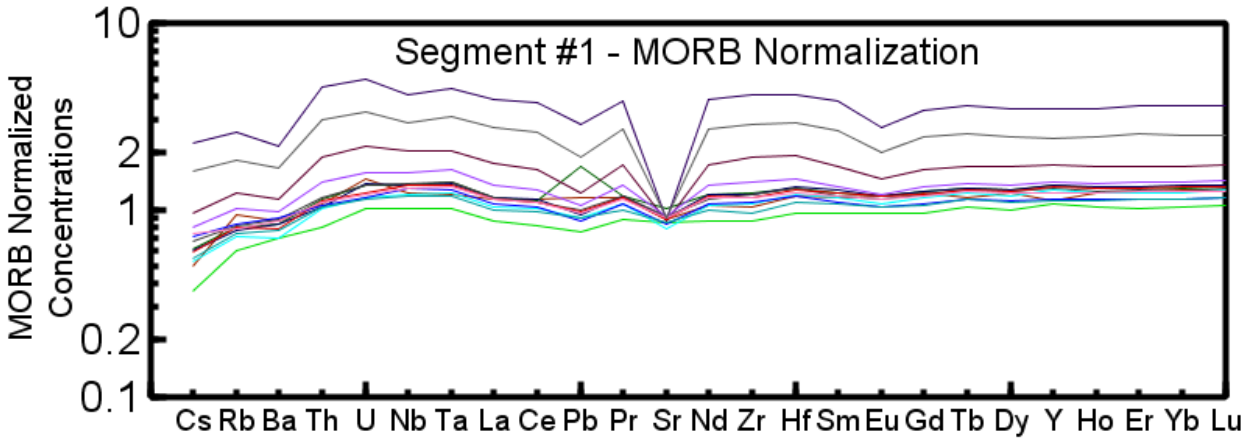
Segment #1 - MORB Normalization
MORB Normalized Concentrations
10
2
1
0.2
0.1
Cs Rb Ba Th U Nb Ta La Ce Pb Pr Sr Nd Zr Hf Sm Eu Gd Tb Dy Y Ho Er Yb Lu

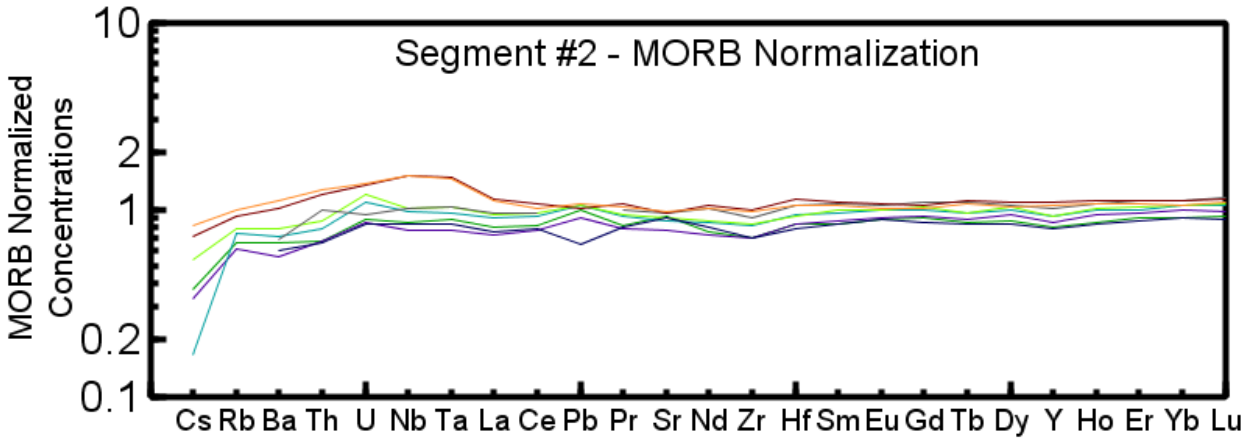
Segment #2 - MORB Normalization
MORB Normalized Concentrations
10
2
1
0.2
0.1
Cs Rb Ba Th U Nb Ta La Ce Pb Pr Sr Nd Zr Hf Sm Eu Gd Tb Dy Y Ho Er Yb Lu

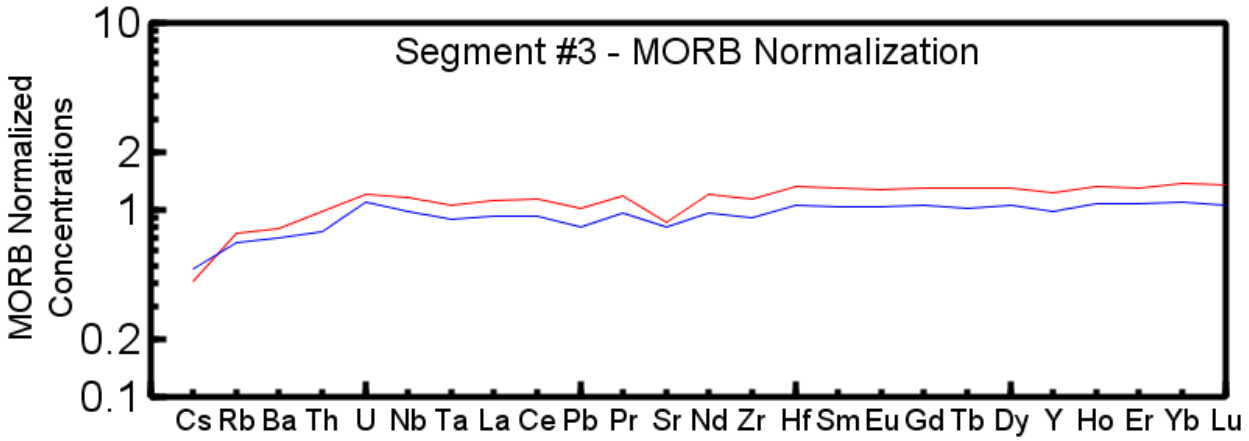
Segment #3 - MORB Normalization
MORB Normalized Concentrations
10
2
1
0.2
0.1
Cs Rb Ba Th U Nb Ta La Ce Pb Pr Sr Nd Zr Hf Sm Eu Gd Tb Dy Y Ho Er Yb Lu

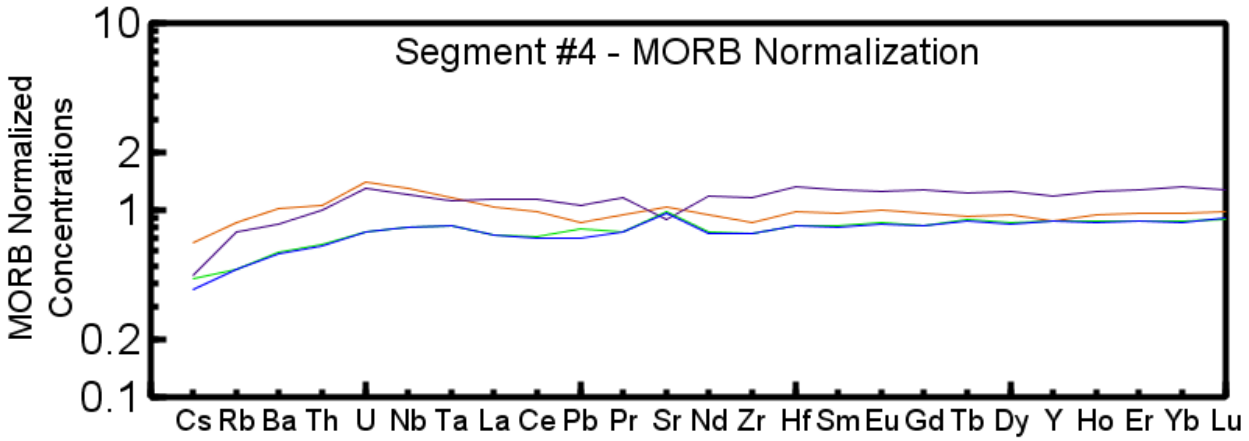
Segment #4 - MORB Normalization
MORB Normalized Concentrations
10
2
1
0.2
0.1
Cs Rb Ba Th U Nb Ta La Ce Pb Pr Sr Nd Zr Hf Sm Eu Gd Tb Dy Y Ho Er Yb Lu

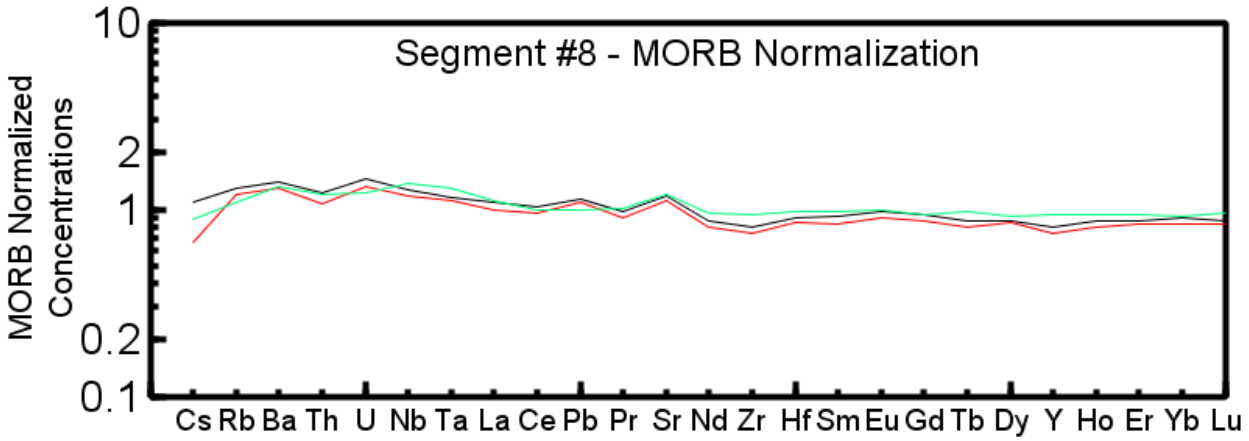
Segment #8 - MORB Normalization
MORB Normalized Concentrations
10
2
1
0.2
0.1
Cs Rb Ba Th U Nb Ta La Ce Pb Pr Sr Nd Zr Hf Sm Eu Gd Tb Dy Y Ho Er Yb Lu

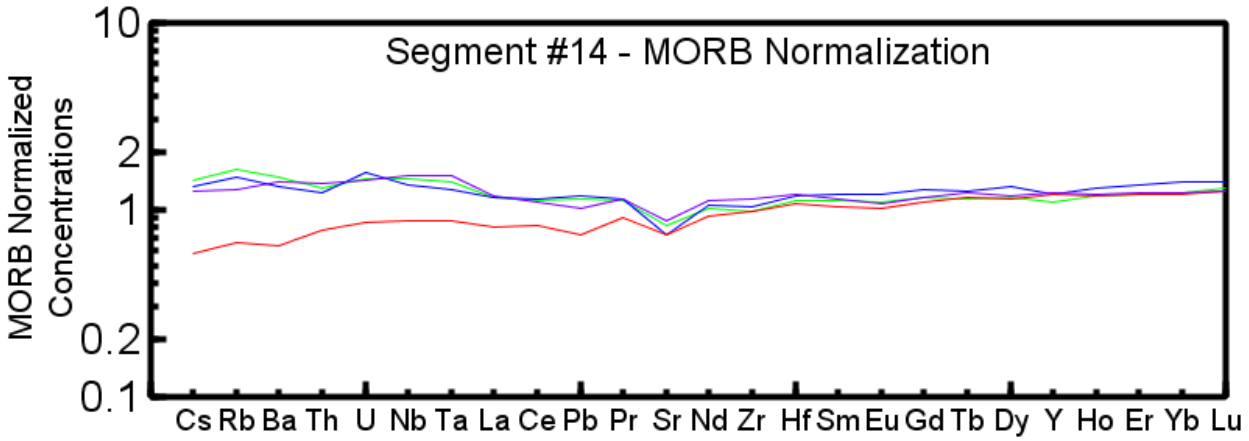
Segment #14 - MORB Normalization
MORB Normalized Concentrations
10
2
1
0.2
0.1
Cs Rb Ba Th U Nb Ta La Ce Pb Pr Sr Nd Zr Hf Sm Eu Gd Tb Dy Y Ho Er Yb Lu

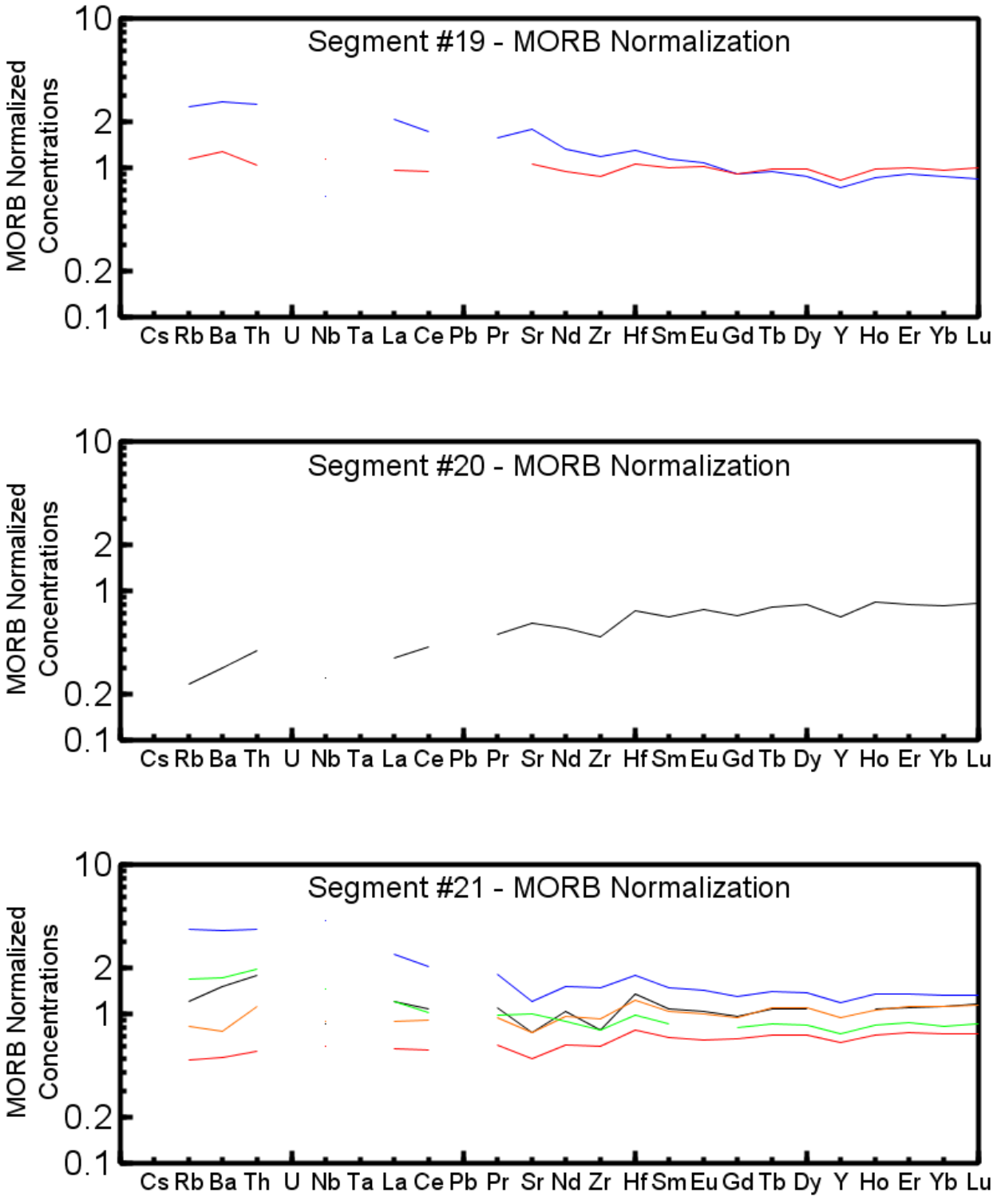

Figure B3. Segmented Gale et al. (2013) trace element data, normalized to NMORB.

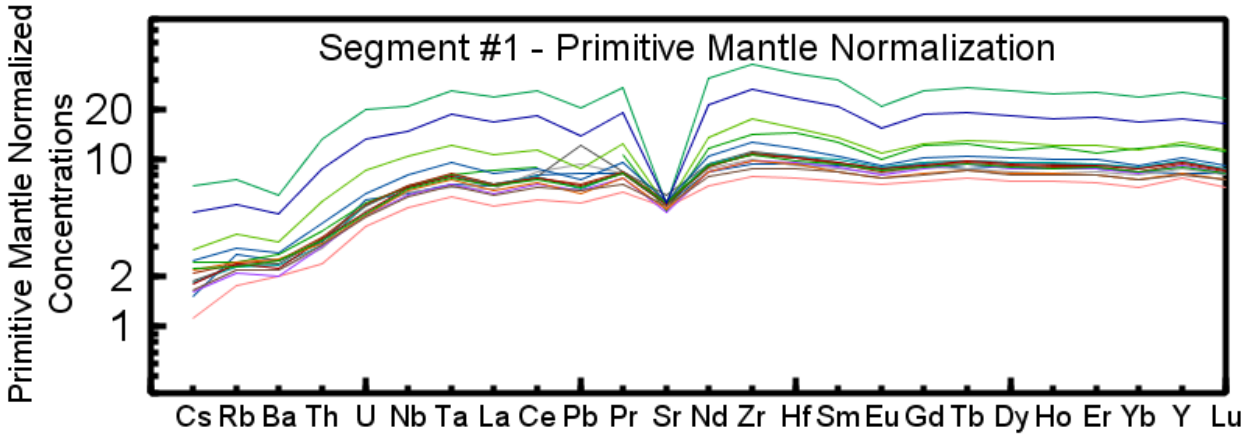
Segment #1 - Primitive Mantle Normalization
Primitive Mantle Normalized Concentrations
20
10
2
1
Cs Rb Ba Th U Nb Ta La Ce Pb Pr Sr Nd Zr Hf Sm Eu Gd Tb Dy Ho Er Yb Y Lu

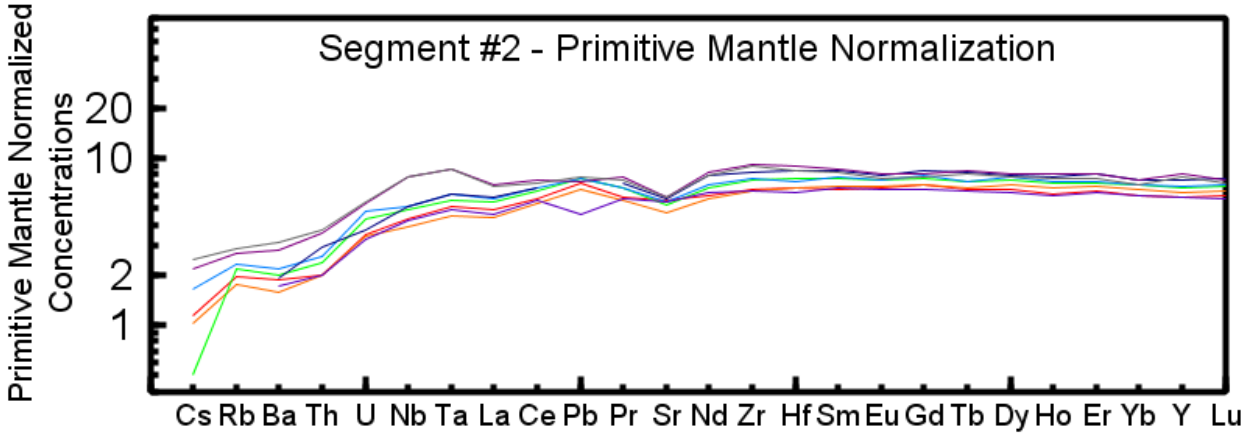
Segment #2 - Primitive Mantle Normalization
Primitive Mantle Normalized Concentrations
20
10
2
1
Cs Rb Ba Th U Nb Ta La Ce Pb Pr Sr Nd Zr Hf Sm Eu Gd Tb Dy Ho Er Yb Y Lu

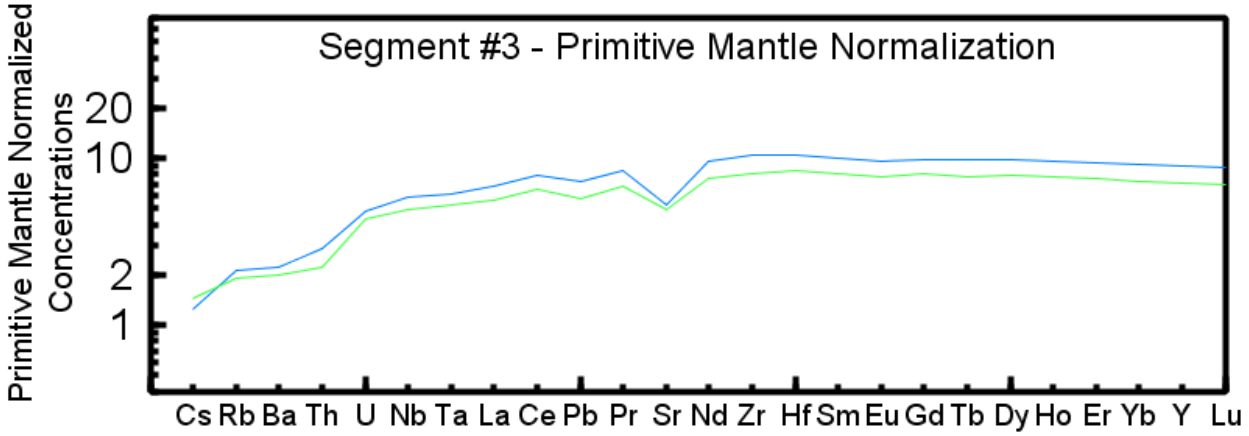
Segment #3 - Primitive Mantle Normalization
Primitive Mantle Normalized Concentrations
20
10
2
1
Cs Rb Ba Th U Nb Ta La Ce Pb Pr Sr Nd Zr Hf Sm Eu Gd Tb Dy Ho Er Yb Y Lu

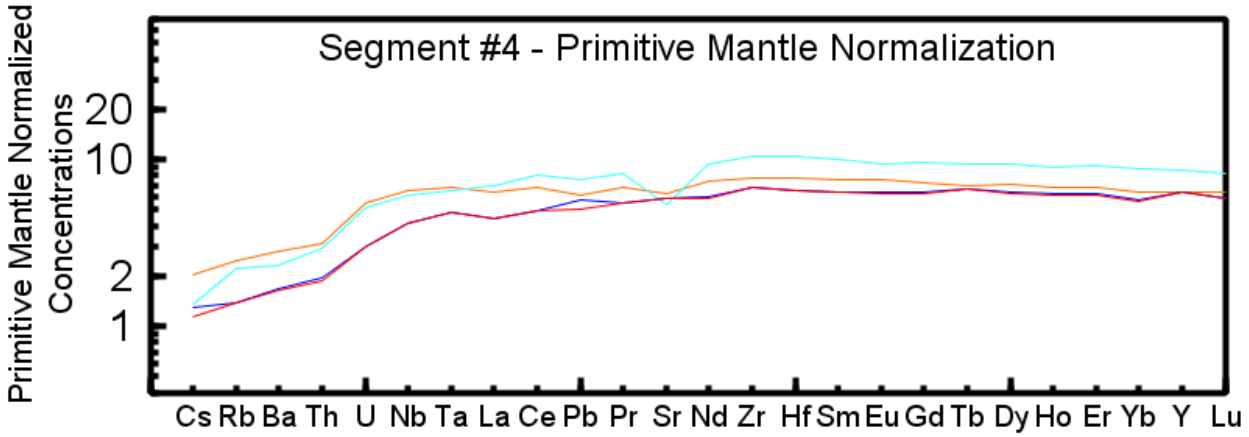
Segment #4 - Primitive Mantle Normalization
Primitive Mantle Normalized Concentrations
20
10
2
1
Cs Rb Ba Th U Nb Ta La Ce Pb Pr Sr Nd Zr Hf Sm Eu Gd Tb Dy Ho Er Yb Y Lu

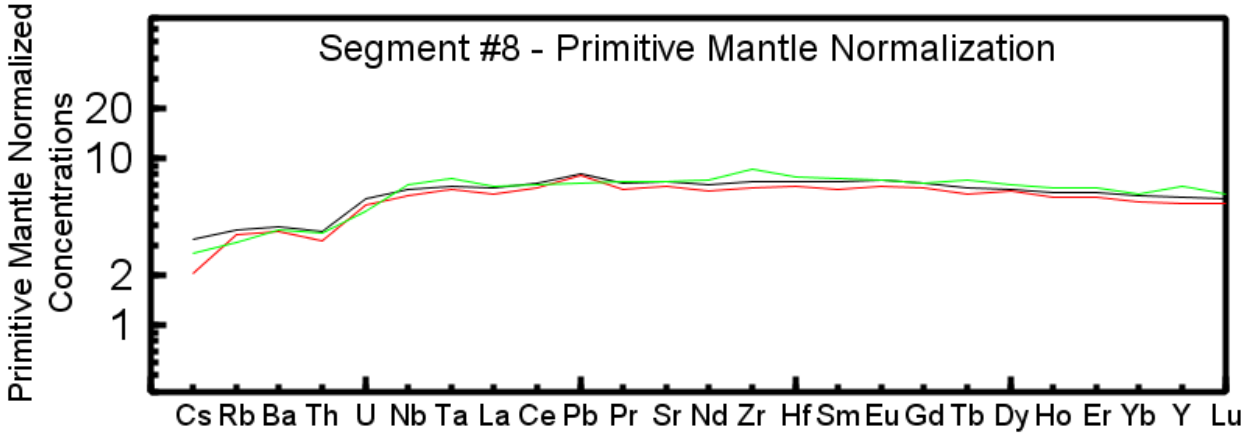
Segment #8 - Primitive Mantle Normalization
Primitive Mantle Normalized Concentrations
20
10
2
1
Cs Rb Ba Th U Nb Ta La Ce Pb Pr Sr Nd Zr Hf Sm Eu Gd Tb Dy Ho Er Yb Y Lu

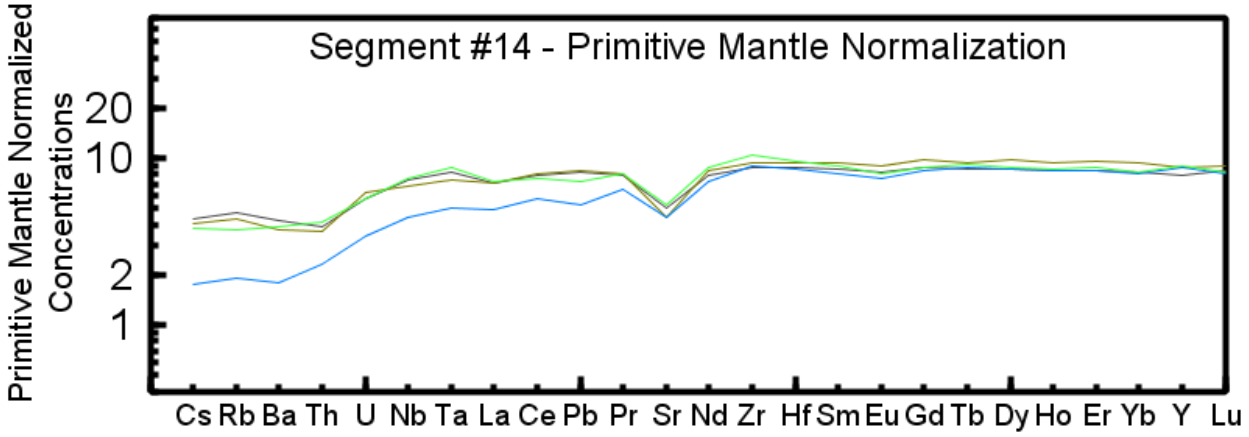
Segment #14 - Primitive Mantle Normalization
Primitive Mantle Normalized Concentrations
20
10
2
1
Cs Rb Ba Th U Nb Ta La Ce Pb Pr Sr Nd Zr Hf Sm Eu Gd Tb Dy Ho Er Yb Y Lu

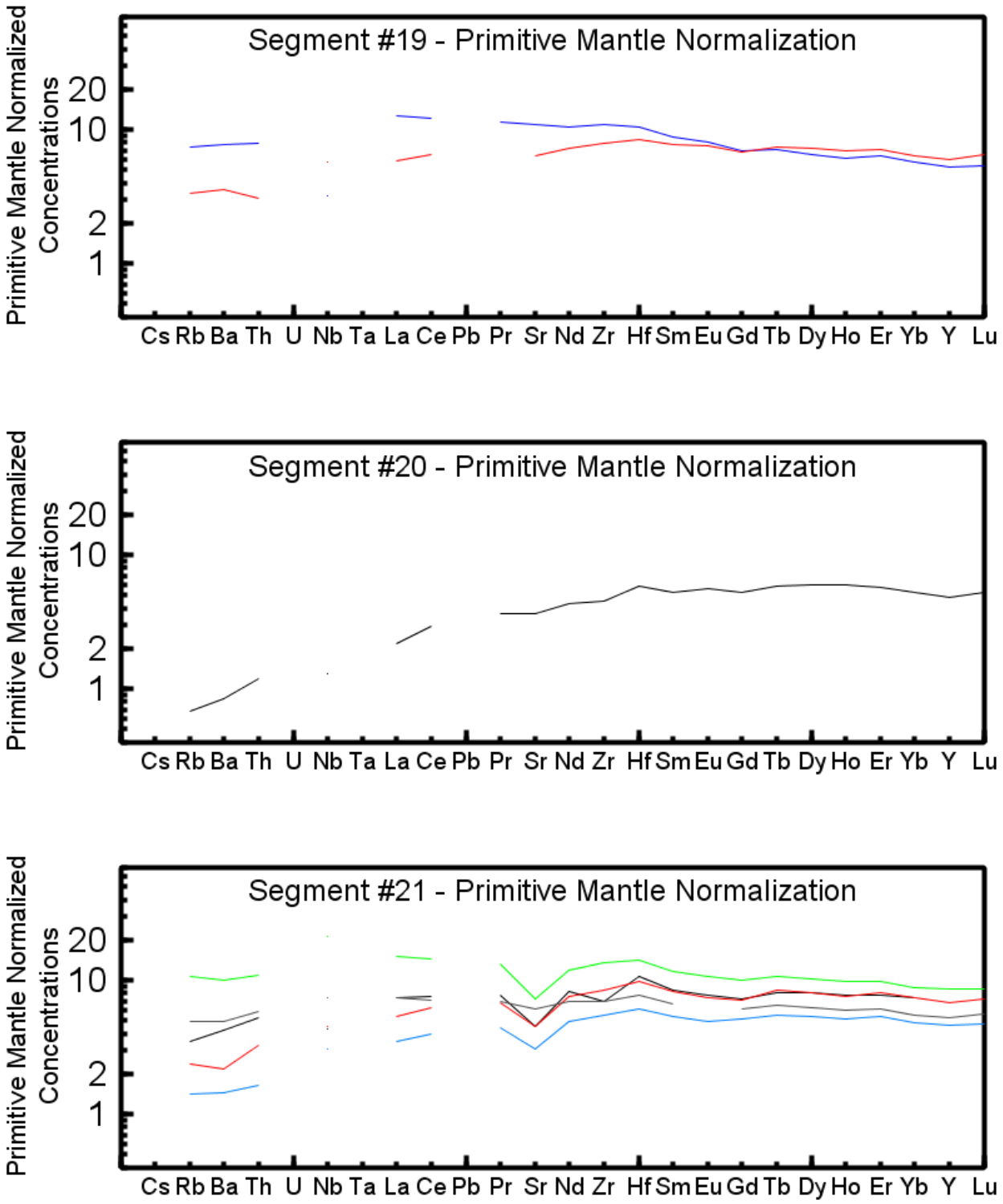

Figure B4. Segmented Gale et al. (2013) trace element data, normalized to Primitive Mantle.

Appendix C: Element Ratio and Na_8 Plots

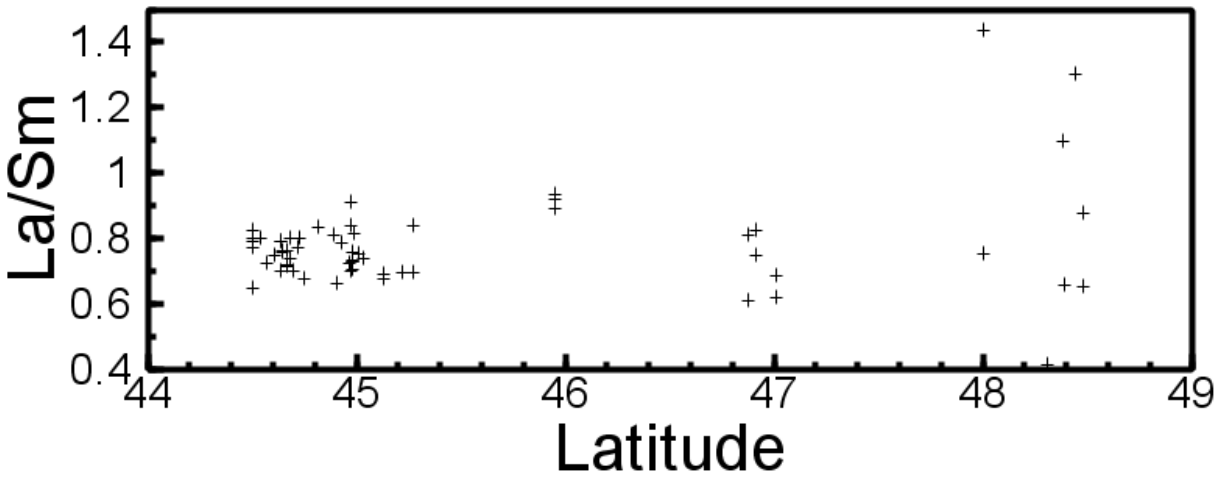

Figure C5. Ratio of La to Sm, plotted against latitude. Data from Gale et al. (2013).

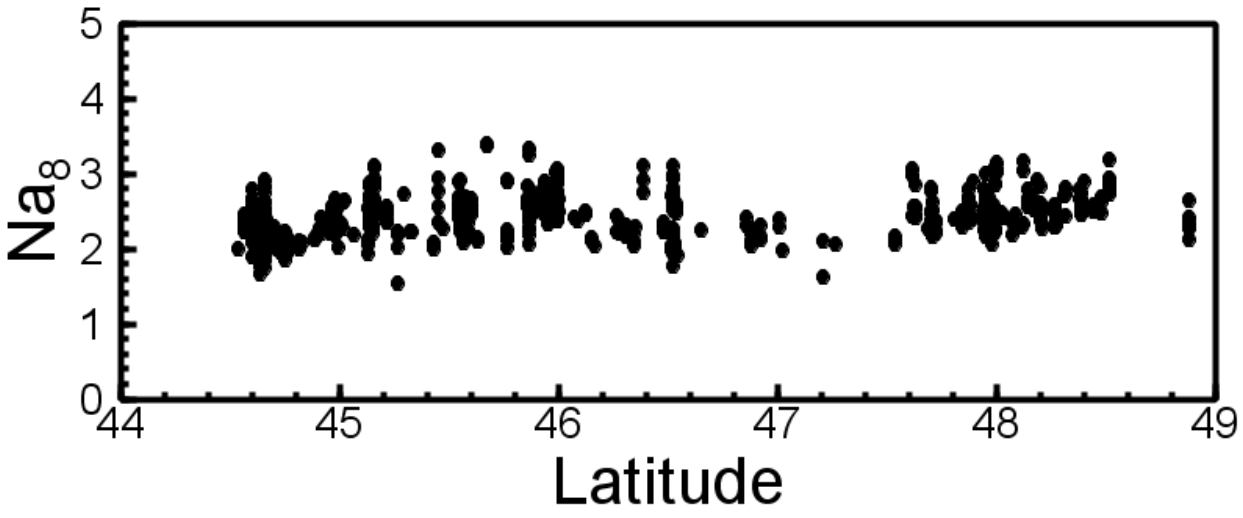

Figure C6. Calculated values of Na_8, from Scott et al. (2012), plotted against latitude.

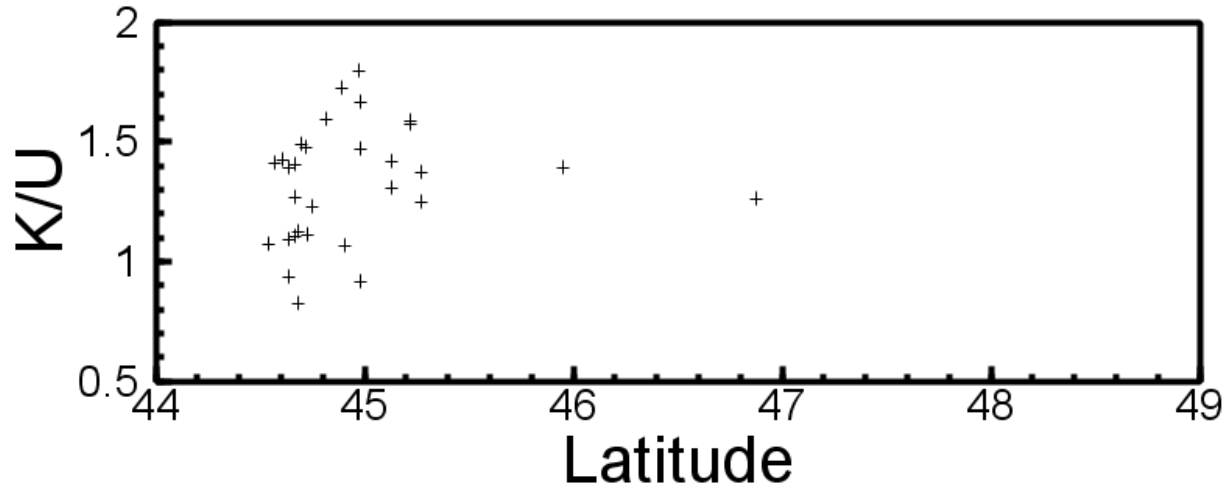

Figure C7. Ratio of K to U, plotted against latitude. Data from Gale et al. (2013).

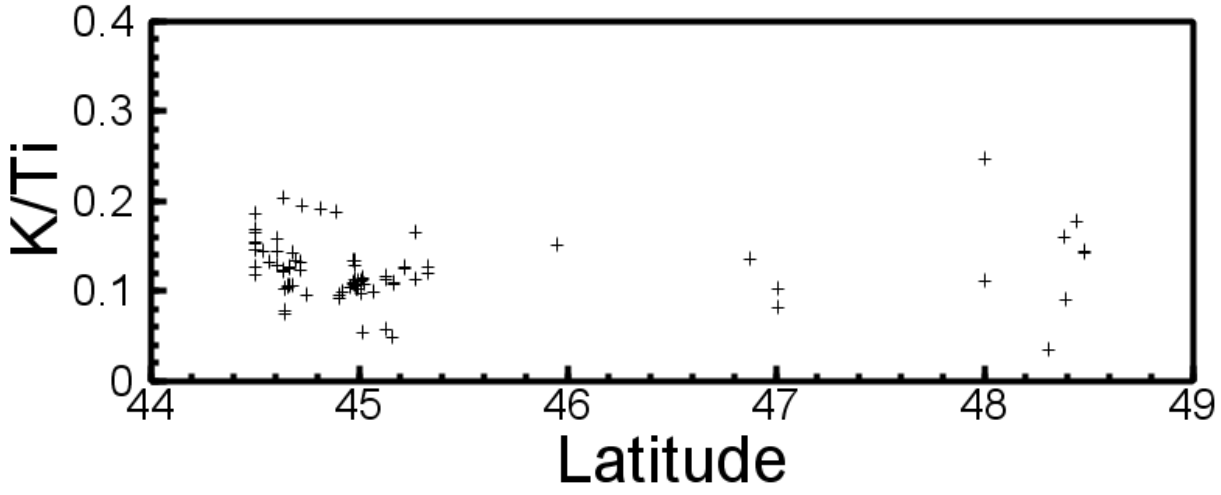

Figure C8. Ratio of K to Ti, plotted against latitude. Data from Gale et al. (2013).

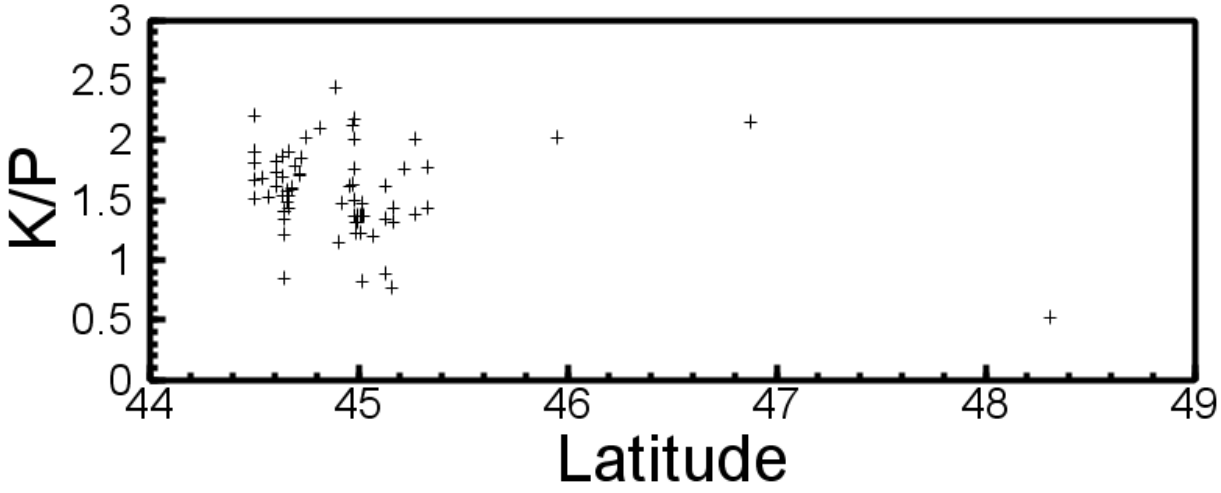

Figure C9. Ratio of K to P, plotted against latitude. Data from Gale et al. (2013).

Appendix D: Trace Element Data

Table D3. Trace element data in ppm, from Gale et al. (2013).

SampleID	Segment	Lat	Lon	Ba	Ce	Cs	Dy	Er	Eu	Gd	Hf	Ho	La	Lu	Nb
NAUBLAN-017-001	1	44.500	-130.400	12.0	10.7		6.2	3.6	1.3	5			3.6		3.7
NAUBLAN-017-002	1	44.500	-130.400	12.0	12		6.1	4.5	1.2				3.9		2.5
NAUBLAN-017-003	1	44.500	-130.400	18.0	14.5		7.3	4.3	1.5	6.1			5		5.2
NAUBLAN-017-004	1	44.500	-130.400	20.0	17		7	4.8	1.5				5.8		4.6
NAUBLAN-017-005	1	44.500	-130.400		14		6.8	3.9	1.5	5.3			5.1		5.8
NAUBLAN-017-006	1	44.500	-130.400		14.5		7.1	4.3	1.5	5.8			5		5.2
NAUBLAN-017-007	1	44.500	-130.400	20.0	19.7		9.5	5.6	1.9	7.8			6.7		5.8
NAUBLAN-017-008	1	44.500	-130.400	16.0	16.5		7.5	5.3	1.5				5.4		4.4
NAUBLAN-017-009	1	44.500	-130.400		16		7.3	4.9	1.6				5.1		3.5
AII84WF-007-004	1	44.540	-130.430	22.4	20.38	0.023	9.247	5.767	1.832	7.468	4.756	1.993	7.373	0.84	7.475
DSC1983-006-002	1	44.570	-130.420	15.2	12	0.013	5.971	3.904	1.31	4.798	2.701	1.325	4.143	0.56	4.264
DSC1983-002	1	44.610	-130.410												
DSC1983-002-001	1	44.610	-130.410	17.1	13.44	0.018	6.678	4.278	1.434	5.384	3.041	1.439	4.764	0.60	4.719
DSC1983-002-002	1	44.610	-130.410												
DSC1983-001-004	1	44.640	-130.420	42.6	46.17	0.054	19.03	12.15	3.483	15.5	10.15	4.088	16.12	1.71	14.79
DSC1983-R006-001	1	44.640	-130.370	13.8	12.46	0.013	6.453	4.195	1.34	5.23	2.931	1.442	4.313	0.61	4.383
AII84WF-002-001	1	44.640	-130.350	19.0	15.76	0.019	7.472	4.762	1.525	6.025	3.57	1.629	5.661	0.68	5.711
ALV2263-006	1	44.642	-130.370	17.1	14.2	0.012	6.71	4.24	1.48	5.53	2.91	1.44	4.75	0.61	4.47
ALV2263-006B	1	44.642	-130.370	41.6											3.4
JdF MORB	1	44.642	229.630	15.1	14.84		6.193	4.024	1.379	5.299	2.808	1.346	4.601	0.59	4.51
ALV2263-008	1	44.643	-130.381												
ALV2263-007	1	44.643	-130.371												4.6
ALV2263-002L	1	44.643	-130.367												3.9
ALV2263-001	1	44.643	-130.366	24.5											3.2
ALV2268-003	1	44.659	-130.365	44.0											4.2
ALV2268-004	1	44.659	-130.365	39.5											5.5
ALV2268-002	1	44.659	-130.360												4.1
ALV1409-001	1	44.670	-130.370	17.2	13.69	0.016	6.819	4.327	1.425	5.508	3.189	1.475	4.849	0.63	4.953
ALV1461-007R	1	44.670	-130.370	16.3	13.98	0.014	7.064	4.534	1.498	5.701	3.249	1.567	4.848	0.65	4.877
AII84WF-012-005	1	44.670	-130.360	15.5	13.61	0.014	6.922	4.437	1.476	5.477	3.124	1.52	4.728	0.64	4.838
ALV1457-001R-C	1	44.680	-130.365	16.5	13.87	0.015	6.996	4.515	1.483	5.651	3.22	1.538	4.874	0.64	4.894
ALV1455-004R	1	44.680	-130.350		20.7	0.032	9.177	5.881	1.811	7.595	4.684	2.015	7.302	0.84	7.396
AII84WF-013-001	1	44.700	-130.340	13.8	10.16	0.009	5.437	3.439	1.192	4.371	2.365	1.211	3.599	0.51	3.682
DSC1983-003-002	1	44.720	-130.340												
DSC1983-003-003	1	44.720	-130.340	17.8	12.72	0.017	6.117	3.911	1.307	4.901	2.895	1.338	4.507	0.56	4.659
DSC1983-C002-001	1	44.730	-130.350												
DSC1983-R002-001	1	44.730	-130.350	32.6	32.14	0.038	13.41	8.617	2.556	11.04	7.116	2.889	11.45	1.21	10.49
OCNGR68-007-VG175	1	44.750	-130.420	18.8	16.1	0.019	8.44	5.26	1.68	7.3	4.46	1.93	5.87	0.83	4.83
DSC1983-005-002	2	44.820	-130.290	22.0	12.65	0.020	5.642	3.644	1.272	4.628	2.606	1.252	4.668	0.53	5.456
DSC1983-009-002	2	44.890	-130.260	19.6	13.26	0.017	5.957	3.841	1.358	4.79	2.791	1.311	4.791	0.55	5.448
ALV2264-002	2	44.905	-130.239	26.9											
ALV2078-004	2	44.909	-130.239	11.0	9.51	0.008	5.15	3.25	1.13	4.16	2.06	1.1	3.06	0.47	2.78
ALV2264-001a	2	44.920	-130.232	31.6											4
ALV2075-001	2	44.930	-130.250	12.0	11		6.2		1.3	5.3			4		
ALV2092-002	2	44.960	-130.212												3.4
ALV2444-001	2	44.963	-130.217		11		5.8	3.5	1.3	4.9		1.3	3.8		
ALV2079-002	2	44.970	229.770	13.4	11.81		5.832	3.828	1.317	5.014	2.601	1.267	4.016	0.56	3.658
ALV2080-001a	2	44.972	-130.212	11.0											6.3
ALV2080-009	2	44.972	-130.212	12.0	11		5.9		1.3	5.1			3.9		
ALV2079-002b	2	44.976	-130.214		12		6.2		1.3	5.3			4.5		
ALV2079-006b	2	44.976	-130.214												5.1
ALV2077-003	2	44.979	-130.208	6.0											3.8
ALV2093-001-A	2	44.980	-130.220	14.0	11.4	0.004	5.41	3.37	1.24	4.51	2.32	1.16	3.74	0.50	3.54
2082-6A	2	44.980	229.780	11.9	9.837		4.566	2.969	1.103	3.853	1.937	0.979	3.185	0.42	3.025

SampleID	Segment	Lat	Lon	Ba	Ce	Cs	Dy	Er	Eu	Gd	Hf	Ho	La	Lu	Nb
ALV2269-001	2	44.983	-130.211	31.1											
ALV2435-004	2	44.983	-130.198		9.6		5	3	1.1	4.1		1.1	3.4		
ALV2435-009b	2	44.983	-130.198		9.8		5.1	3	1.2	4.3		1.1	3.5		
ALV2269-002	2	44.984	-130.203	15.3	11.9	0.013	5.64	3.5	1.25	4.66	2.26	1.19	3.92	0.51	3.64
ALV2269-003	2	44.987	-130.200	20.6											3.6
ALV2442-008	2	44.988	-130.202		9.4		5	3	1.1	4.1		1.1	3.4		
ALV2261-003	2	44.990	-130.201	31.7											
ALV2266-001	2	44.995	-130.198	18.0											4.1
ALV2266-002	2	44.995	-130.198	23.6											
ALV2262-009	2	45.010	-130.189	26.7											
ALV2262-007	2	45.014	-130.191	22.0											4.1
ALV2262-008	2	45.014	-130.191	13.0	10.1	0.009	4.77	3.06	1.11	4.1	2.04	1.01	3.35	0.44	3.07
ALV2262-004	2	45.015	-130.187	26.5											
ALV2262-003	2	45.015	-130.186	24.8											
ALV2432-001	2	45.017	-130.217	26.1											3.9
ALV2432-002	2	45.023	-130.184	24.4											3.8
AII0125-11-020-001	2	45.032	-130.217		12		6	3.7	1.4	5		1.3	4.1		
AII0125-11-011	2	45.068	-130.147	28.7											3.1
YAQ7401-005-003	3	45.130	-130.120	13.8	11.46	0.011	5.799	3.66	1.309	4.794	2.575	1.267	3.838	0.51	3.524
YAQ7401-005-012	3	45.130	-130.120	15.4	14.1	0.010	7.18	4.478	1.606	5.872	3.252	1.563	4.691	0.65	4.186
ALV2430-001	3	45.133	-130.167												3.6
ALV2430-002	3	45.158	-130.135												3.1
AII0125-11-012-A	3	45.170	-130.157	18.3											2.86
AII0125-11-012-B	3	45.170	-130.157	18.9											8.91
ALV1410-002-A	4	45.220	-130.160	11.6	8.806	0.010	4.643	2.971	1.065	3.753	2.023	1.019	3.055	0.43	2.93
ALV1410-003-B	4	45.220	-130.160	11.4	8.773	0.009	4.632	2.942	1.055	3.749	2.028	1.005	3.028	0.43	2.933
YAQ7401-004-002	4	45.270	-130.130	16.3	14.2	0.011	6.872	4.383	1.565	5.76	3.243	1.476	4.776	0.62	4.347
YAQ7401-004-003	4	45.270	-130.130	19.8	12.04	0.016	5.17	3.241	1.259	4.348	2.401	1.101	4.347	0.47	4.676
AII0125-11-018	4	45.328	-130.075												3.86
AII0125-11-017	4	45.333	-130.085	33.7											4.18
ALV1411-001B	8	45.950	-130.020												
ALV1411-001-B	8	45.950	-130.020	26.1	12.29	0.021	5.089	3.181	1.238	4.236	2.393	1.098	4.632	0.45	4.963
XL1723-1A	8	45.950	-130.000	27.2	12.7	0.026	4.8	2.96	1.23	4.24	2.23	1.03	4.54	0.42	4.59
XL1739-2A	8	45.950	-130.000	25.3	11.8	0.016	4.65	2.83	1.13	3.95	2.08	0.95	4.18	0.40	4.29
ALV1415-001-B2-A	14	46.880	-129.280	27.3	13.44	0.030	6.543	4.219	1.36	5.281	2.973	1.42	4.974	0.61	5.435
ALV1415-B005-002	14	46.880	-129.280	12.5	10.11	0.014	6.293	4.083	1.28	5.001	2.648	1.386	3.364	0.59	3.156
ALV2257-001	14	46.910	-129.260	29.3	13.9	0.034	6.4	4.08	1.38	5.22	2.74	1.39	4.88	0.62	5.28
ALV2257-003	14	46.910	-129.260	25.7	14.2	0.032	7.21	4.64	1.5	5.8	2.91	1.53	4.82	0.67	4.87
THO0040-015	14	47.008	-129.300	19.0	14.21		7.7	4.9	1.56	5.48	3.7	1.67	4.79	0.75	3.3
THO0040-017	14	47.008	-129.300		10.81		6.28	4.34	1.28	4.6	3.1	1.37	3.55	0.60	2.3
ENV1986-001-004	19	48.000	-129.167	25.0	11.62		5.34	3.41	1.28	4.07	2.6	1.14	4.02	0.48	4.1
ENV1986-001-005	19	48.000	-129.167	54.0	21.4		4.8	3.07	1.34	4.1	3.2	1	8.74	0.40	2.3
ENV7115-008-001	20	48.310	-129.070	5.9	5.18		4.41	2.77	0.94	3.1	1.8	0.98	1.48	0.39	0.93
TUL1987-011-002	21	48.383	-129.117	34.0	12.49		4.63	2.95		3.66	2.4	0.98	5.03	0.41	5.3
TUL1987-012-005	21	48.392	-129.125	15.0	11.09		5.97	3.83	1.25	4.24	3	1.24	3.68	0.54	3.2
TUL1988-003-001	21	48.445	-129.033	70.0	25.52		7.53	4.65	1.81	5.92	4.4	1.6	10.35	0.64	15.2
TUL1987-006-005	21	48.483	-129.042	29.4	13.42		5.92	3.72	1.3	4.36	3.3	1.26	5.03	0.56	3.1
TUL1987-006-023	21	48.483	-129.042	10.0	7.05		3.94	2.56	0.83	3.06	1.9	0.85	2.41	0.35	2.2

SampleID	Segment	Lat	Lon	Nd	Pb	Pr	Rb	Sm	Sr	Ta	Tb	Th	U	Y	Yb	Zr
NAUBLAN-017-001	1	44.500	-130.400	10.4			1	3.6	111					36.0	3.6	100.0
NAUBLAN-017-002	1	44.500	-130.400	12			1.7		107					38.0	3.8	101.0
NAUBLAN-017-003	1	44.500	-130.400	13.3			1.1	4.1	112					43.0	4.4	126.0
NAUBLAN-017-004	1	44.500	-130.400	15			2.5		121					43.0	4.3	127.0
NAUBLAN-017-005	1	44.500	-130.400	12.6				4	127					40.0	4	117.0
NAUBLAN-017-006	1	44.500	-130.400	13.3				4.2	109					43.0	4.3	129.0
NAUBLAN-017-007	1	44.500	-130.400	18.2			1.4	5.4	107					56.0	5.6	190.0
NAUBLAN-017-008	1	44.500	-130.400	15			1.5		102					48.0	4.7	144.0
NAUBLAN-017-009	1	44.500	-130.400	15					103					46.0	4.7	128.0
AII84WF-007-004	1	44.540	-130.430	18.33	0.619	3.455	2.259	5.96	110	0.498	1.4	0.477	0.181	57.9	5.572	195.0
DSC1983-006-002	1	44.570	-130.420	10.62	0.461	1.967	1.368	3.715	110	0.282	0.924	0.258	0.094	36.7	3.721	97.5
DSC1983-002	1	44.610	-130.410													
DSC1983-002-001	1	44.610	-130.410	12.31	0.484	2.257	1.452	4.134	115	0.32	1.016	0.276	0.099	40.9	4.124	118.2
DSC1983-002-002	1	44.610	-130.410													
DSC1983-001-004	1	44.640	-130.420	41.18	1.445	7.464	4.767	13.17	112	1.061	2.935	1.132	0.416	115.7	11.73	420.4
DSC1983-R006-001	1	44.640	-130.370	11.29	0.457	2.11	1.319	3.993	101	0.293	1.002	0.253	0.096	41.9	4.049	109.8
AII84WF-002-001	1	44.640	-130.350	14.25	0.538	2.655	1.859	4.629	117	0.392	1.137	0.351	0.130	46.9	4.555	142.7
ALV2263-006	1	44.642	-130.370	11.3	0.588	2.27	1.71	4.04	114	0.288	0.95	0.270	0.120	37.1	4.16	105.0
ALV2263-006B	1	44.642	-130.370						112					39.1		125.0
JdF MORB	1	44.642	229.630	12.01	0.662	2.268		3.921	119	0.277	0.954	0.249	0.104	39.6	3.991	110.8
ALV2263-008	1	44.643	-130.381						103					43.2		136.0
ALV2263-007	1	44.643	-130.371						116					37.7		124.0
ALV2263-002L	1	44.643	-130.367				3.1		114					38.4		123.0
ALV2263-001	1	44.643	-130.366				2.2		109					33.8		95.1
ALV2268-003	1	44.659	-130.365						113					38.4		119.0
ALV2268-004	1	44.659	-130.365						106					38.1		121.0
ALV2268-002	1	44.659	-130.360						109					37.9		120.0
ALV1409-001	1	44.670	-130.370	12.13	0.503	2.317	1.507	4.12	117	0.339	1.035	0.291	0.112	42.9	4.121	121.7
ALV1461-007R	1	44.670	-130.370	12.7	0.474	2.337	1.43	4.397	115	0.328	1.066	0.258	0.113	44.4	4.4	121.5
AII84WF-012-005	1	44.670	-130.360	12.53	0.493	2.289	1.486	4.254	113	0.321	1.051	0.281	0.101	44.0	4.325	118.2
ALV1457-001R-C	1	44.680	-130.365	12.73	0.87	2.342	1.47	4.273	130	0.334	1.063	0.284	0.111	44.5	4.293	124.6
ALV1455-004R	1	44.680	-130.350	17.92	0.377	3.383		5.898	116	0.488	1.421	0.545	0.212	57.2	5.744	184.0
AII84WF-013-001	1	44.700	-130.340	9.303	0.389	1.744	1.104	3.319	108	0.243	0.838	0.201	0.084	35.2	3.36	88.7
DSC1983-003-002	1	44.720	-130.340													
DSC1983-003-003	1	44.720	-130.340	11.48	0.439	2.135	1.534	3.777	107	0.308	0.937	0.266	0.096	37.5	3.724	110.3
DSC1983-C002-001	1	44.730	-130.350													
DSC1983-R002-001	1	44.730	-130.350	28.77	0.975	5.3	3.394	9.245	116	0.758	2.075	0.754	0.275	79.0	8.223	292.1
OCNGR68-007-VG175	1	44.750	-130.420	15.79		2.95	1.52	5.62	104	0.327	1.33	0.314	0.114	55.5	5.71	157.1
DSC1983-005-002	2	44.820	-130.290	10.74	0.543	2.033	1.833	3.624	124	0.352	0.876	0.318	0.115	35.2	3.447	99.6
DSC1983-009-002	2	44.890	-130.260	11.2	0.511	2.121	1.696	3.825	123	0.353	0.913	0.305	0.112	36.5	3.658	101.6
ALV2264-002	2	44.905	-130.239				2.2		102					30.4		85.5
ALV2078-004	2	44.909	-130.239	7.8	0.457	1.55	1.12	2.99	99	0.184	0.72	0.170	0.071	28.3	3.23	71.1
ALV2264-001a	2	44.920	-130.232						104					32.3		91.6
ALV2075-001	2	44.930	-130.250					3.3							3.6	
ALV2092-002	2	44.960	-130.212						111					33.8		106.0
ALV2444-001	2	44.963	-130.217	9.8				3.4							3.4	
ALV2079-002	2	44.970	229.770	10.72		1.961		3.709	122	0.25	0.892	0.248	0.078	33.6	3.677	92.5
ALV2080-001a	2	44.972	-130.212						114					33.5		107.0
ALV2080-009	2	44.972	-130.212					3							3.5	
ALV2079-002b	2	44.976	-130.214					3.2							3.6	
ALV2079-006b	2	44.976	-130.214						118					34.0		107.0
ALV2077-003	2	44.979	-130.208						109					33.6		102.0
ALV2093-001-A	2	44.980	-130.220	8.99	0.533	1.82	1.38	3.33	111	0.229	0.78	0.200	0.091	30.3	3.43	82.8
2082-6A	2	44.980	229.780	8.485	0.33	1.584		2.92	114	0.202	0.687	0.169	0.069	26.3	2.941	70.9

SampleID	Segment	Lat	Lon	Nd	Pb	Pr	Rb	Sm	Sr	Ta	Tb	Th	U	Y	Yb	Zr
ALV2269-001	2	44.983	-130.211						120					29.9		85.9
ALV2435-004	2	44.983	-130.198	8.7				2.9							3	
ALV2435-009b	2	44.983	-130.198	8.9				3.1							3	
ALV2269-002	2	44.984	-130.203	9.31	0.539	1.84	1.46	3.46	116	0.249	0.79	0.220	0.100	30.7	3.42	85.1
ALV2269-003	2	44.987	-130.200						115					28.7		86.9
ALV2442-008	2	44.988	-130.202	8.3				2.7							3	
ALV2261-003	2	44.990	-130.201						115					27.4		79.7
ALV2266-001	2	44.995	-130.198						112					29.0		82.3
ALV2266-002	2	44.995	-130.198						113					27.6		79.1
ALV2262-009	2	45.010	-130.189						113					29.7		83.7
ALV2262-007	2	45.014	-130.191				2		113					27.1		80.8
ALV2262-008	2	45.014	-130.191	8.07	0.505	1.62	1.23	2.88	117	0.211	0.7	0.170	0.073	26.7	2.97	72.2
ALV2262-004	2	45.015	-130.187						121					27.4		78.7
ALV2262-003	2	45.015	-130.186						118					28.1		78.7
ALV2432-001	2	45.017	-130.217						113					31.2		109.0
ALV2432-002	2	45.023	-130.184				2.3		114					27.4		106.0
AII0125-11-020-001	2	45.032	-130.217	11				3.6							3.7	
AII0125-11-011	2	45.068	-130.147				1.97		121					31.6		97.1
YAQ7401-005-003	3	45.130	-130.120	10.18	0.41	1.881	1.218	3.596	103	0.213	0.835	0.190	0.090	32.2	3.556	91.2
YAQ7401-005-012	3	45.130	-130.120	12.86	0.516	2.327	1.359	4.476	110	0.252	1.065	0.244	0.100	40.8	4.529	116.3
ALV2430-001	3	45.133	-130.167				2.1		112					28.5		84.7
ALV2430-002	3	45.158	-130.135						117					34.5		109.0
AII0125-11-012-A	3	45.170	-130.157				1.02		120					26.8		73.9
AII0125-11-012-B	3	45.170	-130.157				1.45		119					26.0		73.4
ALV1410-002-A	4	45.220	-130.160	8.064	0.402	1.508	0.873	2.844	123	0.198	0.719	0.164	0.063	29.0	2.831	76.3
ALV1410-003-B	4	45.220	-130.160	7.903	0.36	1.496	0.882	2.811	122	0.197	0.711	0.160	0.063	28.7	2.781	75.3
YAQ7401-004-002	4	45.270	-130.130	12.68	0.531	2.297	1.401	4.433	113	0.268	1.011	0.248	0.107	39.2	4.311	116.9
YAQ7401-004-003	4	45.270	-130.130	9.962	0.432	1.855	1.566	3.352	132	0.277	0.756	0.264	0.116	28.8	3.151	86.6
AII0125-11-018	4	45.328	-130.075						119					31.1		93.0
AII0125-11-017	4	45.333	-130.085				2.43		114					30.2		92.1
ALV1411-001B	8	45.950	-130.020													
ALV1411-001-B	8	45.950	-130.020	10.11	0.506	1.993	2.005	3.364	154	0.313	0.8	0.300	0.101	31.1	3.008	95.3
XL1723-1A	8	45.950	-130.000	9.32	0.573	1.94	2.37	3.2	152	0.279	0.71	0.310	0.120	26.5	2.97	81.5
XL1739-2A	8	45.950	-130.000	8.57	0.56	1.8	2.21	2.9	142	0.267	0.66	0.270	0.110	24.5	2.72	75.1
ALV1415-001-B2-A	14	46.880	-129.280	11.84	0.517	2.239	2.359	3.984	110	0.364	0.995	0.348	0.119	40.6	4.046	116.6
ALV1415-B005-002	14	46.880	-129.280	9.796	0.371	1.782	1.211	3.575	93	0.208	0.956	0.195	0.071	39.9	3.955	100.1
ALV2257-001	14	46.910	-129.260	10.7	0.579	2.19	3.01	3.84	105	0.336	0.93	0.330	0.120	35.9	4.04	98.9
ALV2257-003	14	46.910	-129.260	11.3	0.602	2.23	2.72	4.16	93	0.305	1.02	0.310	0.130	40.2	4.6	106.0
THO0040-015	14	47.008	-129.300	13.23		2.44	1.9	4.52	97		1.14	0.290		40.0	4.67	121.0
THO0040-017	14	47.008	-129.300	10.29		1.89		3.7	80		0.91	0.250		33.0	4.32	93.0
ENV1986-001-004	19	48.000	-129.167	9.89			2.1	3.45	134		0.8	0.260		27.0	3.11	88.0
ENV1986-001-005	19	48.000	-129.167	14.12		3.11	4.7	3.94	230		0.77	0.670		24.0	2.83	121.0
ENV7115-008-001	20	48.310	-129.070	5.9		1	0.43	2.31	77		0.63	0.100		22.0	2.57	50.0
TUL1987-011-002	21	48.383	-129.117	9.48		1.92	3.1	2.96	128		0.7	0.500		24.0	2.69	78.0
TUL1987-012-005	21	48.392	-129.125	10.18		1.87	1.5	3.62	96		0.9	0.280		31.0	3.64	94.0
TUL1988-003-001	21	48.445	-129.033	16.19		3.63	6.7	5.13	154		1.15	0.920		39.0	4.36	152.0
TUL1987-006-005	21	48.483	-129.042	11.07		2.15	2.2	3.71	96		0.88	0.450			3.66	78.0
TUL1987-006-023	21	48.483	-129.042	6.59		1.21	0.9	2.39	64		0.59	0.140		21.0	2.39	61.0

Appendix E: Major Oxide Data

Table E4. Major oxide data in wt. %, from Gale et al. (2013).

SampleID	Segment	Lat	Lon	SiO_2	TiO_2	FeO_t	MgO	Al_2O_3	CaO	Na_2O	K_2O	P_2O_5	MnO
NAUBLAN-017-001	1	44.500	-130.400	50.09	1.55	10.75	7.76	14.62	11.89	2.43	0.14	0.16	0.19
NAUBLAN-017-002	1	44.500	-130.400	50.02	1.54	10.81	7.56	14.68	12.03	2.36	0.17	0.17	0.21
NAUBLAN-017-003	1	44.500	-130.400	50.41	1.92	11.88	6.93	13.83	11.47	2.45	0.20	0.20	0.21
NAUBLAN-017-004	1	44.500	-130.400	49.82	1.86	11.29	7.27	14.68	11.53	2.39	0.22	0.22	0.21
NAUBLAN-017-005	1	44.500	-130.400	50.45	1.83	11.65	7.09	13.97	11.26	2.60	0.22	0.19	0.21
NAUBLAN-017-006	1	44.500	-130.400	50.49	1.83	11.78	7.23	13.75	11.34	2.49	0.19	0.20	0.21
NAUBLAN-017-007	1	44.500	-130.400	51.07	1.88	11.88	6.47	13.72	11.06	2.62	0.25	0.25	0.21
NAUBLAN-017-008	1	44.500	-130.400	50.26	1.77	11.47	7.00	14.12	11.86	2.53	0.15	0.19	0.21
NAUBLAN-017-009	1	44.500	-130.400	50.40	1.71	11.43	7.04	14.00	11.90	2.43	0.19	0.20	0.22
AII84WF-007-004	1	44.540	-130.430	50.34	2.23	13.19	6.09	13.55	10.39	2.93	0.23	0.26	
DSC1983-006-002	1	44.570	-130.420	50.05	1.67	11.04	7.63	14.31	11.60	2.71	0.16	0.20	
DSC1983-002	1	44.610	-130.410	50.36	1.94	12.22	6.78	13.86	10.85	2.78	0.22	0.23	0.22
DSC1983-002-001	1	44.610	-130.410	50.27	1.84	11.78	7.40	14.03	11.00	2.64	0.17	0.20	
DSC1983-002-002	1	44.610	-130.410	50.50	1.93	12.32	6.71	13.88	10.80	2.72	0.20	0.22	
DSC1983-001-004	1	44.640	-130.420	50.80	3.14	16.26	3.42	12.02	7.84	3.55	0.46	0.47	
DSC1983-R006-001	1	44.640	-130.370	49.74	1.79	11.67	7.93	14.15	11.30	2.42	0.16	0.18	
AII84WF-002-001	1	44.640	-130.350	50.22	1.93	11.99	6.97	13.80	11.11	2.92	0.17	0.21	
ALV2263-006B	1	44.642	-130.370	50.32	1.93	12.25	6.70	13.86	11.35	2.63	0.14	0.19	0.21
ALV2263-008	1	44.643	-130.381	50.19	2.12	13.07	6.35	13.46	11.28	2.51	0.12	0.19	0.33
ALV2263-007	1	44.643	-130.371	50.28	1.90	12.24	6.76	13.95	11.24	2.68	0.14	0.19	0.21
ALV2263-002L	1	44.643	-130.367	50.37	1.92	11.99	6.78	13.99	11.39	2.61	0.14	0.20	0.19
ALV2263-001	1	44.643	-130.366	50.15	1.51	10.71	7.50	14.61	12.31	2.42	0.08	0.18	0.21
ALV2268-003	1	44.659	-130.365	50.40	1.86	12.12	6.75	14.13	11.12	2.65	0.14	0.18	0.23
ALV2268-004	1	44.659	-130.365	50.16	1.88	11.91	7.07	14.12	11.31	2.57	0.14	0.17	0.25
ALV2268-002	1	44.659	-130.360	50.37	1.83	11.92	7.03	14.12	11.32	2.48	0.14	0.17	0.21
ALV1409-001	1	44.670	-130.370	49.97	1.86	12.00	7.09	13.94	11.20	2.87	0.17	0.21	
ALV1461-007R	1	44.670	-130.370	50.07	1.97	12.38	7.09	13.77	11.02	2.71	0.15	0.20	
AII84WF-012-005	1	44.670	-130.360	50.14	1.90	12.32	6.90	13.80	11.13	2.78	0.17	0.17	
ALV1457-001R-C	1	44.680	-130.365	50.26	1.98	12.27	6.93	13.71	11.08	2.80	0.15	0.18	
ALV1455-004R	1	44.680	-130.350	50.49	2.05	12.55	6.48	13.69	10.57	2.96	0.21	0.25	
AII84WF-013-001	1	44.700	-130.340	49.92	1.55	10.70	7.74	14.47	12.19	2.50	0.15	0.16	
DSC1983-003-002	1	44.720	-130.340	49.73	1.89	11.67	7.44	14.14	11.52	2.55	0.18	0.20	
DSC1983-003-003	1	44.720	-130.340	50.18	1.90	11.72	7.25	14.00	11.48	2.43	0.17	0.19	
DSC1983-R002-001	1	44.730	-130.350	50.84	2.59	14.23	5.17	12.92	9.26	3.23	0.36	0.37	
OCNGR68-007-VG175	1	44.750	-130.420	50.93	2.46	14.21	5.88	13.36	10.81	2.63	0.17	0.16	
DSC1983-005-002	2	44.820	-130.290	49.94	1.60	10.87	7.94	14.42	11.77	2.32	0.22	0.20	
DSC1983-009-002	2	44.890	-130.260	50.18	1.71	11.28	7.41	14.16	11.52	2.57	0.23	0.18	
ALV2264-002	2	44.905	-130.239	50.35	1.32	10.41	7.70	14.81	12.31	2.31	0.09	0.15	0.21
ALV2078-004	2	44.909	-130.239	50.06	1.38	10.44	7.81	14.99	12.20	2.35	0.09	0.15	
ALV2264-001a	2	44.920	-130.232	50.03	1.42	10.25	7.80	15.07	12.36	2.30	0.10	0.13	0.20
ALV2092-002	2	44.960	-130.212	50.56	1.46	10.58	7.51	14.63	12.08	2.39	0.11	0.13	0.19
ALV2079-002	2	44.970	229.770	49.93	1.74	11.03	7.43	14.50	12.00	2.48	0.17	0.15	
ALV2080-001a	2	44.972	-130.212	50.13	1.53	10.57	7.53	15.15	11.76	2.49	0.12	0.14	0.20

SampleID	Segment	Lat	Lon	SiO_2	TiO_2	FeO_t	MgO	Al_2O_3	CaO	Na_2O	K_2O	P_2O_5	MnO
ALV2079-006b	2	44.976	-130.214	50.27	1.51	10.55	7.66	14.83	11.85	2.49	0.12	0.14	0.20
ALV2077-003	2	44.979	-130.208	49.66	1.50	10.48	7.52	15.81	11.79	2.42	0.12	0.13	0.19
ALV2093-001-A	2	44.980	-130.220	50.17	1.67	11.06	7.52	14.40	11.62	2.63	0.16	0.14	
2082-6A	2	44.980	229.780	49.97	1.49	10.05	7.75	15.20	12.27	2.34	0.14	0.13	
ALV2269-001	2	44.983	-130.211	50.19	1.31	9.90	7.92	15.10	12.40	2.42	0.10	0.14	0.18
ALV2269-002	2	44.984	-130.203	50.50	1.43	10.78	7.33	14.47	12.08	2.57	0.11	0.14	0.23
ALV2269-003	2	44.987	-130.200	50.09	1.22	9.84	8.00	15.26	12.45	2.39	0.09	0.13	0.20
ALV2261-003	2	44.990	-130.201	49.98	1.23	10.00	8.03	15.19	12.50	2.34	0.09	0.14	0.17
ALV2266-001	2	44.995	-130.198	49.95	1.26	10.01	7.91	15.12	12.61	2.32	0.10	0.14	0.23
ALV2266-002	2	44.995	-130.198	50.04	1.23	10.07	7.93	15.10	12.59	2.32	0.09	0.13	0.17
ALV2262-009	2	45.010	-130.189	49.89	1.29	10.12	7.91	15.03	12.62	2.36	0.09	0.14	0.20
ALV2262-007	2	45.014	-130.191	50.17	1.25	10.01	7.72	15.12	12.52	2.37	0.10	0.14	0.24
ALV2262-004	2	45.015	-130.187	50.23	1.24	10.17	7.71	14.90	12.58	2.41	0.10	0.14	0.17
ALV2262-003	2	45.015	-130.186	50.41	1.23	10.36	7.58	14.69	12.48	2.46	0.10	0.13	0.22
ALV2432-001	2	45.017	-130.217	49.09	1.55	10.53	7.77	15.50	12.22	2.66	0.06	0.14	0.17
ALV2432-002	2	45.023	-130.184	49.33	1.29	10.64	7.86	15.12	12.33	2.67	0.10	0.14	0.18
AII0125-11-011	2	45.068	-130.147	50.23	1.40	10.93	7.31	14.54	12.33	2.44	0.10	0.16	0.21
YAQ7401-005-003	3	45.130	-130.120	49.72	1.74	11.37	7.53	14.10	12.14	2.44	0.14	0.20	
YAQ7401-005-012	3	45.130	-130.120	50.03	2.02	12.38	6.87	13.84	11.26	2.55	0.17	0.20	
ALV2430-001	3	45.133	-130.167	48.97	1.46	10.59	7.91	15.79	12.09	2.54	0.06	0.13	0.17
ALV2430-002	3	45.158	-130.135	49.42	1.74	10.75	7.94	14.87	12.05	2.55	0.06	0.15	0.19
AII0125-11-012-A	3	45.170	-130.157	50.07	1.14	9.37	8.13	15.69	12.49	2.35	0.09	0.12	0.21
AII0125-11-012-B	3	45.170	-130.157	50.00	1.16	9.35	8.34	15.57	12.47	2.36	0.09	0.13	0.20
ALV1410-002-A	4	45.220	-130.160	49.58	1.31	9.73	8.61	15.20	12.24	2.52	0.12	0.13	
ALV1410-003-B	4	45.220	-130.160	49.97	1.32	9.70	8.42	15.29	12.14	2.35	0.12	0.13	
YAQ7401-004-002	4	45.270	-130.130	49.81	1.97	12.11	7.04	13.95	11.51	2.55	0.16	0.22	
YAQ7401-004-003	4	45.270	-130.130	50.06	1.60	10.56	7.70	14.80	11.72	2.51	0.19	0.18	
AII0125-11-018	4	45.328	-130.075	50.55	1.42	10.61	7.34	14.51	12.21	2.47	0.13	0.14	0.22
AII0125-11-017	4	45.333	-130.085	50.56	1.40	10.69	7.32	14.49	12.19	2.47	0.12	0.16	0.22
ALV1411-001-B	8	45.950	-130.020	49.52	1.55	11.05	7.39	14.68	12.10	2.72	0.17	0.16	
ALV1415-001-B2-A	14	46.880	-129.280	50.13	1.84	11.77	7.32	14.33	11.11	2.48	0.18	0.16	
THO0040-015	14	47.008	-129.300	49.98	2.18	12.44	6.87	13.45	11.24	2.80	0.16		0.25
THO0040-017	14	47.008	-129.300	50.51	1.71	11.60	7.45	13.66	11.77	2.48	0.10		0.22
ENV1986-001-004	19	48.000	-129.167	50.63	1.63	9.08	7.80	14.82	12.10	3.04	0.13		0.19
ENV1986-001-005	19	48.000	-129.167	49.50	1.80	8.67	7.80	15.83	11.69	3.22	0.32		0.19
ENV7115-008-001	20	48.310	-129.070	50.29	1.22	9.65	8.23	14.66	12.75	2.60	0.03	0.11	0.21
TUL1987-011-002	21	48.383	-129.117	49.88	1.22	8.33	8.94	15.51	12.75	2.43	0.14		0.20
TUL1987-012-005	21	48.392	-129.125	49.43	1.71	10.25	8.36	15.28	11.62	2.51	0.11		0.21
TUL1988-003-001	21	48.445	-129.033	49.90	2.37	11.54	6.41	14.18	10.99	3.19	0.30		0.18
TUL1987-006-005	21	48.483	-129.042	50.34	2.07	11.03	6.94	13.84	11.47	3.10	0.21		0.26
TUL1987-006-023	21	48.483	-129.042	50.56	1.84	10.93	6.87	14.21	11.63	2.93	0.19		0.14